Weather Effects in Energy Seasonal Adjustment: An Application to France Energy Consumption*

Marie Bruguet[†,1,2,3], Arthur Thomas [‡,1,3], and Ronan Le Saout[§4]

[1]Université Paris-Dauphine, Université PSL, LEDa, CNRS, IRD, 75016 Paris, France
[2]Commissariat Général au Développement Durable, SDES, 92700, Puteaux, France
[3]Climate Economics Chair, 75001, Paris, France
[4]Université de Rennes, ENSAI, CREST, F-35000 Rennes, France

January 30, 2025

Abstract

This paper addresses the challenge of adjusting energy consumption data for weather variations by introducing a novel General Weather Indicator (GWI). The GWI combines multiple weather variables, including temperature, wind, sunlight, rain, and cloudiness, using a novel econometric approach that applies K-means for threshold identification and LASSO for variable selection. Through an empirical analysis of sectoral, electricity and natural gas consumption in France, we demonstrate that the GWI outperforms the standard HDD approach by addressing three main concerns: the lack of statistical criteria for defining the base temperature, the reliance solely on temperature as the weather variable, and the assumption of a constant base temperature over time and space. Based on these results, we propose an analysis of the sectoral functional form and an estimation of weather elasticities for energy demand in France at both monthly and daily levels.

JEL classification: C32, E61, P28, Q47

Keywords: sectoral energy consumption, seasonal adjustment, weather,heating degree days, k-means clustering, penalization

*We warmly thank Virginie Andrieux, Marie Bessec, Anna Creti, Tomás Del Barrio Castro and Daniel Herrera Araujuo for their insightful suggestions and detailed comments. We would also like to thank the participants of the seminars and conferences of the International Association for Applied Econometrics (IAAE 2024), the 2024 RCEA International Conference in Economics, Econometrics, and Finance (ICEEF 2024) and the 44th International Symposium on Forecasting (ISF) and of the workshop organised by the French section of the Association of Energy Economists (FAEE) for their valuable comments. The views expressed in this paper are solely those of the authors and do not necessarily reflect those of the institutions with which they are affiliated.

[†]email: marie.bruguet@dauphine.eu
[‡]email: arthur.thomas@dauphine.psl.eu
[§]email: ronan.le-saout@ensai.fr

1 Introduction

In the context of climate change, the Paris Agreement calls for a reduction in global emissions to mitigate its effects. In 2021, energy use accounted for 76.7% of total emissions on average for Europe, highlighting the significant potential for European countries to meet their emissions targets by significantly reducing energy consumption.[1] In this context, the French government has decided reduce energy consumption by 20% in 2030 compared to 2012 (see MTE, 2020). This initiative aims to reduce both greenhouse gas emissions and dependence on fossil fuels. In order to assess the effectiveness of such strategies, government agencies need relevant indicators to control for weather variations in the energy demand. Otherwise, a change in temperature or an increase in wind episodes could be misinterpreted as a change in energy demand in response to a policy of demand reduction.

This paper focuses on identifying and analysing meteorological factors that influence energy consumption. It is evident that there is a significant correlation between monthly energy consumption and temperature. This is largely due to the high energy demand for heating buildings during the winter months and cooling buildings in hot climates during the summer. To ensure reliable comparisons over time and to assess the impact of socio-economic factors alone, it is essential to correct observed consumption for seasonality and weather variations (see e.g. Pang et al., 2022). It is therefore important for public policy makers to have access to robust seasonal adjustments. For example, in France, this weather- and seasonally-adjusted energy consumption serves as a benchmark for assessing progress toward the net-zero goal of the national strategy (*"Stratégie Nationale Bas-Carbone"*). Futhermore, all indicators used to monitor and inform future energy capacity investment decisions are expressed in weather- and seasonally-adjusted values, in line with the government's ten-year plan.[2] It is also crucial to assess the impact of a sufficiency policy such as the *"Plan de sobriété énergétique"* on energy consumption, taking into account weather and seasonal variations.[3] This is particularly relevant in the context of a change in consumer behavior due to environmental awareness and/or price increases, such as the inflationary spike triggered by the sharp fall in Russian supplies.[4]

The concept of Heating Degree Days (HDD) and Cooling Degree Days (CDD) has traditionally been used to explain seasonal patterns in energy consumption due to weather variations. The calculation of HDD (CDD) is based on the concept of base temperature. This indicator is only calculated if the temperature at time t is below (or above) the base temperature. The base temperature is the outdoor temperature at which agents begin to heat

[1] National emissions reported to the United Nations Framework Convention on Climate Change and the EU Greenhouse Gas Monitoring Mechanism.

[2] The *"Programmation Pluriannuel de l'Energie"* Multi-Annual Energy Plan (MAEP) establishes the priorities for government action on energy policy for metropolitan France over the next decade, divided into two 5-year periods. The current plan covers the period from 2024 to 2033.

[3] *"Plan de sobriété énergétique"* promotes the concept of energy sufficiency, which is the voluntary and organized reduction of energy consumption. It includes various measures aimed at changing certain habits and reducing unnecessary energy consumption.

[4] Environmental awareness has been growing in France over the years, and an annual survey by the Agence de l'Environnement et de la Maîtrise de l'Energie (ADEME) assesses a 36% awareness of climate change as the main environmental concern ADEME (2022)

(cool) buildings to achieve an indoor comfort temperature. The concept of HDD (CDD) is based on the understanding that there is a non-linear relationship between temperature and energy consumption, as outlined by Henley and Peirson (1997). This methodology dates back to the 1870s when it was first used in agricultural yield studies. It is now widely used to measure adjusted energy use. While there has been extensive research on the estimation of temperature response functions for energy demand (see Fazeli et al., 2016, for a comprehensive review), a broader view of the literature (De Azevedo et al., 2015) underlines the need for a statistically validated approach, as most papers using HDD indicators still define a base temperature of 18°C, mostly based on Thom (1954).[5]

Beyond the choice of base temperature, this definition of HDD (CDD) can be challenged in three ways: first, there is no reason for the base temperature to be constant over time. Studies such as Sailor and Pavlova (2003) and Kennard et al. (2022) emphasize the rise in the level of CDD links to climate change, however, it is also important to account for dynamic base temperatures when predicting future energy demand. These changes in base temperature may arise from factors such as increased awareness of energy efficiency, advancements in building insulation technologies, and shifts in comfort preferences, all of which could be influenced by climate change. Second, there is no reason for the base temperature to be constant in space, as Bessec and Fouquau (2008) underscores the limitations of assuming a uniform base temperature across different geographical regions. Finally, there is no reason to take temperature as the sole weather indicator. Atalla et al. (2018); Lundström (2017); Staffell et al. (2023) broaden the scope to include other weather indicators in the literature, highlighting the multifaceted nature of weather factors influencing energy consumption, including consideration of the effects of wind and sunlight.

Building on this literature and relying on a statistical approach to select weather variables, we propose a new general weather indicator (GWI). We define GWI, as a vector of the optimal linear combination of heating days variable (HDV) and cooling days variable (CDV) of different weather variables among temperature, wind, sunlight duration, rain and cloudiness. To construct this indicator we proposed a two-step procedure: First, for each variable, we extract the optimal(s) threshold(s) that capture the non-linear relationship between the energy consumption and this variable using K-means. To our knowledge, this is the first time that K-means has been used to extract these thresholds. Compared to the standard likelihood-based thresholding approach, the K-means approach is more flexible: one does not need to specify a priori a functional form, between the energy consumption and the weather variable and/or the number of regimes before proceeding with the estimation. In our particular case, we also found that the K-means approach leads to an estimate that is more robust to spatial heterogeneity. Then, in a second step, the GWI is constructed by selecting, for each energy consumption e.g. natural gas and electricity, the optimal linear combination of these HDV and CDV using a LASSO penalization. We put forward the optimal specification in the sample according to different criteria: likelihood-based and prediction error-based. As an application of our approach, we studied electricity and natural gas consumption in France, disaggregated by delivery mode.[6] This disaggregation allows us to proxy different sectoral

[5]See Appendix A.1 for a complete literature review.

[6]Electricity and natural gas consumption account for 44% of total French final energy consumption. Both consumptions are considered in the empirical analysis of this paper, assuming that natural gas and electricity

activities from residential and services to heavy industry. We use both monthly and daily energy consumption series: the monthly data span from January 2012 to December 2022, and the daily low voltage energy consumption series span from January 2019 to December 2022. Weather data are provided at a fine spatial scale, with either daily or monthly frequency, depending on the indicator.

We find that, for any energy consumption type considered, the GWI is a linear combination of temperature HDV and sunlight HDV. Notably, for medium-voltage electricity, which serves as a proxy for tertiary consumption, wind HDV and temperature CDV are also included. For temperature HDV, we determined that the optimal base temperature is 15°C, for low-voltage natural gas and electricity, regardless of the inclusion of other weather variables. This deviates from both the value currently used in French national statistics (17°C), the one recommended by the European statistical agency Eurostat, and the standard value in the literature (18°C). Regarding other economic sectors, our results show that, at a monthly aggregated level, none of the CDVs are significant except for temperature in the functional form of medium-voltage electricity demand, highlighting the role of air conditioning in the tertiary sector. For the industrial sector, we found that the response function of electricity consumption to weather conditions is much weaker than for other sectors. This is largely because energy consumption depends on production processes unrelated to the need for heating or cooling, in this specific sector. Additionally, we examine the relationship between temperature and energy demand, focusing on two concepts: comfort zone and felt temperature. First, comfort zone is defined as the range of temperatures within which economic agents do not feel the need to adjust their environment through heating or cooling, leading to stable energy consumption. Second, we find that wind and sunlight duration, alongside temperature, are important weather control variables for the residential sector. Thus, felt temperature appears to have a greater influence on heating behavior than measured temperature itself. As a byproduct of our results, we also estimate sectoral thermosensitivity for French energy consumption at both monthly and daily levels.

We perform several checks to ensure the robustness of the GWI indicator, addressing the three main criticisms commonly associated with standard HDD measures. First, we challenge the standard HDD, and the GWI indicator in a rolling time windows analysis. We found that the standard HDD based benchmarks are never selected against the GWI base temperature. Second, we test the robustness of the threshold estimation to spatial aggregation on residential electricity consumption: we study the 12 administrative regions of France, covering a wide range of different climatic zones. We found that our approach is robust to spatial aggregation, indeed we recover the same national threshold by averaging the one from each region, but we obtain different regional values in line with the variability of the French climatic zones. We also found cooling behavior (CDV on temperature) to be significant for residential electricity consumption in one southern region of France, highlighting the role of air conditioning in this region. Finally, we test the sensitivity of the GWI approach to time aggregation, still on residential electricity consumption, we study and compare daily and monthly frequency consumption. We find a greater significance of felt temperature compared

consumption react differently to weather variations. For example, it is unusual to use natural gas to cool buildings in summer. In addition, the proposed approach could be extended to other energy sources such as coal, oil, and biomass, but this is beyond the scope of this paper.

to measured temperature also at the daily frequency.

The remainder of this paper is organized as follows. In Section (2), we present the energy consumption data, weather data, and associated descriptive statistics. Section (3) describes the methodological procedure used to construct the GWI. In Section (4), we develop our main application, focusing on defining the country's base temperature and analyzing the role of other weather variables using monthly aggregated data. Further, in Section (4), we also discuss the economic implications of our new estimation by analyzing the functional form of France's energy demand, introducing the concepts of the comfort zone and felt temperature. We then propose new estimates of thermosensitivity of the energy demand by sector. In Section (5), we conduct a series of robustness tests to demonstrate that the GWI addresses the three main concerns of the HDD. We evaluate the GWI against various benchmarks over time through a rolling time-window analysis at the monthly aggregated level, as well as using daily data, and across regions with spatially disaggregated data. Finally, a concluding section (6) is proposed.

2 Preliminary analysis of the data

2.1 Energy consumption

Since one of the goals of this paper is to develop a robust time series adjustment framework to facilitate accurate monitoring of the impact of national policies aimed at reducing energy consumption, our main application focuses on the monthly aggregated gas and electricity consumption time series at the French national level, initially named $[\mathbf{q}_t^{gas}]$ and $[\mathbf{q}_t^{elec}]$, respectively. The final consumption of electricity is divided into three series according to the type of distribution. First, the low-voltage one, denoted $[\mathbf{q}_t^{Low_e}]$, is defined as a response to the demand of households and small businesses, providing power to everyday appliances with a level voltage between 0.23 kV and 0.40 kV. Second, medium one, denoted $[\mathbf{q}_t^{Med_e}]$, is described as a distribution made to facilitate the local transport of electricity to small industries, SMEs and businesses with a level tension between 15 kV and 30 kV. Thirdly, high voltage one, denoted as $[\mathbf{q}_t^{High_e}]$, for a voltage level ranging from 63 kV to 400 kV.

Natural gas energy consumption is decomposed into two series of final consumption, namely: the distributed one denoted $[\mathbf{q}_t^{Low_g}]$, defined as a network that transports gas from transmission networks to final consumers not directly connected to transmission networks. The transported one, denoted by $[\mathbf{q}_t^{High_g}]$, denotes networks that facilitate the import of gas from terrestrial interconnections with neighbouring geographical areas and methane terminals. These monthly energy consumption series can be used as a proxy for the energy demand of the three main economic sectors: Industrial, Tertiary and Residential, for easier economic interpretation, as described in Table 1.[7] This database is publicly available, we mainly used data that span from January 2012 to December 2022 (132 observations) from the *Service des Données et Etudes Statistiques* (SDES).[8]

[7] See Table 14 for the sectoral distribution of each delivered energy type and Table 15 for the distribution of total consumption across all different sectors in Appendix A.2

[8] Catalogue of energy data in France - *https://www.statistiques.developpement-durable.gouv.fr*

Table 1: Time series of energy consumptions by economic sector

Series		Sector	Share
Electricity - Low voltage	$q_t^{Low_e}$	Proxy for residential consumption	(80%)
Electricity - Medium voltage	$q_t^{Med_e}$	Proxy for tertiary consumption	(58%)
Electricity - High voltage	$q_t^{High_e}$	Proxy for industrial consumption	(81%)
Gas - Distributed	$q_t^{Low_g}$	Proxy for residential, tertiary and small industry consumption	(74%)
Gas - Transported	$q_t^{High_g}$	Proxy for industrial consumption, gas-fired power plant included	(94%)

Notes: Residential consumption represents 80% of the total electricity demand delivered via low voltage i.e. 80% share.

We also examine French residential electricity consumption at daily frequency and with regional distribution.[9] These daily electricity demand series for low voltage ($<$ 36kVA) are available from January 1, 2019, to December 31, 2022 from Enedis (1,461 observations). We checked that the aggregate daily frequency consumption have the same distribution than the monthly frequency one, at the source is not the same (see Table 17). The regional level is characterized by the study of the 12 metropolitan administrative regions of France, with the exception of *Corse*: *Auvergne-Rhône-Alpes, Bourgogne-France-Comté, Bretagne, Centre-Val de Loire, Grand Est, Hauts-de-France, Île-de-France, Normandie, Nouvelle-Aquitaine, Occitanie, Pays de la Loire, Provence-Alpes-Côte d'Azur*.[10] The electricity consumption of these administrative regions is made available by Enedis only from January 1, 2022, to December 31, 2023 (730 observations by region).

2.2 Weather data

Weather data are provided by the official French weather and climate service *Météo France* at a daily or monthly frequency, depending on the indicators.[11] These data are available at a fine spatial scale, as they are monitored by 539 weather stations throughout metropolitan France. In line with the literature (see for example Kennard et al., 2022), each weather station is weighted daily according to the population of the last available French census. The weighting is used to reflect the population level and the associated level of heating and cooling demand. In fact, the energy demand for a given temperature differs between countries according to their respective population densities, as highlighted by Kennard et al. (2022). It is important to note that the weighting by population census is particularly effective for the residential sector. However, it can result in the emergence of spatial heterogeneity on a more granular level for the tertiary and industrial sectors. For these sectors, weighting by the number of people in employment may be seen as more appropriate. However, we test these alternative weighting methods, such as employment-based weighting for industrial and service sectors, and the results showed no significant differences in the weighted temperature distributions, as confirmed by Wilcoxon significance tests.[12] However, given the sensitivity of the residential sector to weather conditions, we maintain the population-based weighting for this general study. First, each administrative town in France is associated with the

[9] Natural gas consumption is not available at daily frequency

[10] Figure 14 shows the location of each administrative region on the map of mainland France.

[11] Catalogue of meteorological data in France - *https://meteo.data.gouv.fr/*

[12] See appendix B.1 for a comparison between weights sources.

nearest weather station, i.e. a station can be associated with several towns, but each town is associated with only one station. Then, the sum of the population of each one is added to the corresponding station, giving each station a certain population weight. Finally, the daily weather indicators are weighted as follows

$$weather_s(pop) = \frac{weather_s * pop_s}{\sum_{i=1}^{s} pop_i}$$

Where s is one of the 539 stations in the area, pop_s is the population associated with the station and $\sum_{i=1}^{s} pop_i$ is the national population.

Based on the literature (Dell et al., 2014; Lundström, 2017), five different initial weather indicators are chosen, see Table 2. The cloudiness [**cloudiness**] is measured as the number of days in a month where the share of the cloudy sky is greater than or equal to 80%, the rainfall [**rain**] is measured as the amount of rainfall in 24 hours (millimeters), the temperature [**temp**] is measured as the mean temperature in 24 hours (degrees Celsius), the sunlight [**sunlight**] is measured as the sunshine duration (minutes), and finally, the wind speed [**wind**] is measured as the daily average of 10-minute periods during which the wind speed at 10 meters above the ground is recorded (meters per second). It is important to note that the term sunshine duration is used to describe the length of time during which the ground surface is irradiated by direct solar radiation. This duration can be considered an indicator of the frequency of *favourable weather conditions*. Consequently, it not only reflects the difference in sunshine duration due to the Earth's rotation, but also takes into account days, even in summer, when solar radiation does not directly irradiate the ground surface due to overcast skies.

Table 2: Weather time-series

Series		**Units (/24h)**
Cloudiness	*cloud*	Number of days per month with overcast > 80%
Rain	*rain*	Rain level in millimeters
Temperature	*temp*	Average temperature in °C
Sunlight	*sunlight*	Duration of sunshine in minutes
Wind	*wind*	Wind speed in m/s

2.3 Descriptive statistics

Figure 1-(a), displays the monthly aggregated natural gas consumption in France $\mathbf{q}_t^{gas}$, with the part due to the distributed $\mathbf{q}_t^{Low_g}$ and the transported $\mathbf{q}_t^{High_g}$. The data indicates a seasonal pattern in natural gas consumption, primarily due to the distributed portion. Figure 1-(b), displays the monthly aggregated electricity in France $\mathbf{q}_t^{elec}$, with contributions from low voltage $\mathbf{q}_t^{Low_e}$, medium voltage $\mathbf{q}_t^{Med_e}$, and high voltage $\mathbf{q}_t^{High_e}$. It reveals a similar seasonal pattern, mainly driven by low voltage demand.[13] In the Appendix A.3, we show that this similar seasonal pattern appears at the daily frequency for electricity (see Figure 12 in Appendix A.3).

[13]These seasonal patterns are confirmed by the analysis of the autocorrelation function (ACF) available Figure 11 in Appendix A.3

Figure 1: Sectoral energy demand time-series

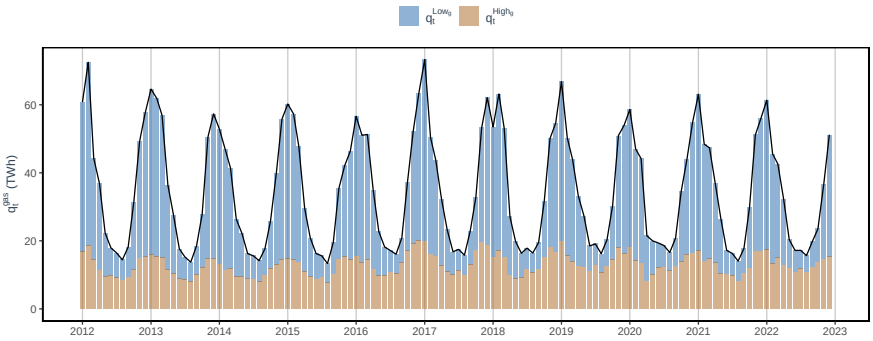

(a)

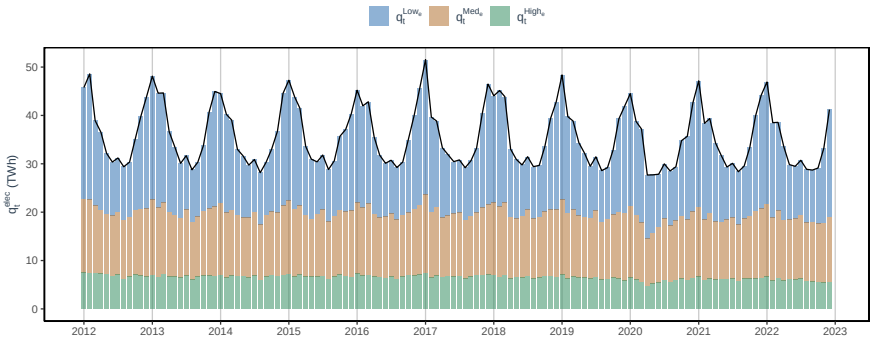

(b)

Notes : Cummulative distribution in time for electricity demand into $q_t^{Low_e}$, $q_t^{Med_e}$ and $q_t^{High_e}$ and for gas demand into $q_t^{Low_g}$ and $q_t^{High_g}$. Monthly energy demand data span the period from January 2012 to December 2022.

Table 3 shows the correlation between the selected energy consumption time series and the five initial weather indicators. There is a strong correlation between monthly energy consumption and temperature because of the large amount of energy needed to heat buildings in winter. However, other weather indicators may also correlate with energy consumption. This simple correlation exercise shows weaker correlations for cloudiness and rain. Temperature has a strong negative correlation with energy demand, about -0.96 and -0.91 for total gas and electricity consumption, respectively. Sunlight has a similar relationship, with a correlation of -0.83 and -0.79 with total gas and electricity consumption, respectively. However, sunlight is also strongly correlated with the level of temperature, so these indicators may carry a similar signal. Wind speed also has a significant positive correlation at the monthly level, meaning that an increase in wind speed leads to more energy demand, which can be due to air infiltration of buildings, as highlighted in the literature (Sherman, 1987; Sinnott, 2016). The correlation with total gas and electricity consumption is around 0.53 and 0.46 respectively.

At the sectoral disaggregated level, the correlations reveal two main singular behaviors. First, $q_t^{High_e}$ exhibits very weak correlations with weather factors, including temperature. This aligns with the expectation of non-significant weather-related variations in electricity consumption from the industrial sector. In this sector, the share of heating using electricity is assumed to be minimal, as electricity is predominantly used for production processes that are largely independent of weather conditions. A visual inspection of the relationship between $q_t^{High_e}$ and temperature supports this notion (see Figure 2-(c)). Second, the correlation with temperature is notably weaker for $q_t^{Med_e}$ than for other energy types and sectors. This can be attributed to a symmetric effect between heating and cooling behaviors, where both positive and negative correlations are observed. However, the negative effect dominates, resulting in an overall negative correlation (see Figure 2-(b)). These findings underscore the potential limitations of a correlation-based approach when the relationship between variables is strongly non-linear and highlight the necessity for a robust methodology.

Table 3: Correlation between weather and energy time series

	temp	**sunlight**	**wind**	**rain**	**cloudiness**
$q_t^{Low_g}$	-0.969	-0.825	0.556	0.112	-0.020
	(0.000)	(0.000)	(0.000)	(0.063)	(0.739)
$q_t^{High_g}$	-0.822	-0.764	0.331	0.069	-0.057
	(0.000)	(0.000)	(0.000)	(0.252)	(0.345)
$q_t^{Low_e}$	-0.934	-0.807	0.498	0.130	0.008
	(0.000)	(0.000)	(0.000)	(0.031)	(0.896)
$q_t^{Med_e}$	-0.410	-0.324	0.031	-0.064	0.435
	(0.000)	(0.000)	(0.608)	(0.292)	(0.000)
$q_t^{High_e}$	-0.012	-0.043	0.164	0.044	-0.017
	(0.848)	(0.479)	(0.006)	(0.465)	(0.782)
q_t^{gas}	-0.966	-0.833	0.531	0.107	-0.027
	(0.000)	(0.000)	(0.000)	(0.075)	(0.656)
q_t^{elec}	-0.916	-0.790	0.466	0.100	0.134
	(0.000)	(0.000)	(0.000)	(0.097)	(0.026)

Notes : The table shows the correlation coefficients and the p-values associated. The columns are ranked according to the level of correlation.The p-values represent the probability that the null hypothesis, which represents a null correlation, is non-rejected. Thus a null p-value is interpreted as a correlation significantly different from 0. The variablesq_t^{gas} andq_t^{elec} represent the sums of the respective variables $q_t^{Low_g}$, $q_t^{High_g}$ and $q_t^{Low_e}$,$q_t^{Med_e}$,$q_t^{High_e}$. The data are at a monthly frequency, spanning from January 2000 to December 2022.

Then, the weather data correlation with energy is also available at the daily frequency in Table 18 in Appendix A.3, mainly confirm the results from Table 3. The temperature is the main driver for energy demand but, as highlighted in Table 3, the amount of sunlight or the wind speed are also correlated and could influence the consumption, and should be considered in the pool of possible weather indicators that influence energy consumption.

3 Methodology

In this section, we present our proposed framework for adjusting energy consumption to seasonal and weather variations.

3.1 Seasonal adjustment

To construct seasonally adjusted statistics, accounting for both working-day effects and weather variations, the recommended econometric approach is based on regSARIMA methodology.[14] While the regressive component includes a set of regressors explaining both working-day effects and weather variations, the SARIMA component of the model is tailored to extract the seasonal patterns from the remaining variations in the regression stage. This model can be summarized as follows:

$$\begin{cases} q_t = \beta GWI_{q_t} + \beta_2 ly_t + \beta_3 wd_t + \beta_4 D_{03-2020} + x_t \\ \Phi(B^s)\delta(B^s)x_t = \Theta(B^s)a_t \end{cases} \tag{1}$$

Equation (1) describes the model with q_t the time series to be adjusted, ly_t is a vector of dummy variables accounting for the leap year in the specification, wd_t are two related variables accounting for working days, $D_{03-2020}$ is a transitory shock that accounts for the COVID-19 crisis, and GWI_t is the general weather indicator defined in section 3.2.2. This indicator may include more than one climate variable, and thus the estimated β may be a vector of parameters.[15]

The second part of the model is derived from the seasonal term of the x_t residuals and is defined by the SARIMA process, along a parameter denoted S, which takes $S = 12$ in a monthly setup. SARIMA can be decomposed into two stationary polynomials, the autoregressive $\Phi(B^s)$ and the moving average $\delta(B^s)$, and then into a nonstationary polynomial, the difference process $\Theta(B^s)$. The variations of the series that are not explained by the regressors nor by the SARIMA process are reflected in the last term a_t, in other words, a_t can be described as the adjusted time series following a $N(\mu_a, \sigma_a^2)$ distribution centered around μ_a, the mean monthly energy demand. The estimation of the model (1) is done by maximum likelihood with the function *X13* from Quartier-La-Tente et al. (2024).

3.2 Weather adjustement

Traditionally, the concepts of Heating Degree Days (HDD) (2) and Cooling Degree Days (CDD) (3) have been adopted as a solution to explain the seasonal patterns of energy demand due to weather variations. The calculation of CDD is based on the concept of base

[14] This approach is recommended by Eurostat. The European agency is responsible for developing, producing, and disseminating European statistics. It sets and enforces statistical standards, methods, and procedures, ensuring the production of comparable data across the European Union for various audiences. Eurostat's role is defined in Article 6 of Regulation (EC) No 223/2009 of the European Parliament and of the Council of March 11, 2009, on European Statistics.

[15] In this specification, it is worth noting that the term GWI_t is centred around the so-called Null Unified Days indicators, which is the average of past GWIs over two decades.

temperature, the indicator is calculated if and only if the temperature at time t is below (above) the base temperature. This method dates back to the 1870s in studies of agricultural yields and is now widely used to measure adjusted energy demand.

$$HDD = \begin{cases} T_{base} - T_t \; if \; T_t < T_{base} \\ 0 \; otherwise \end{cases} \tag{2}$$

$$CDD = \begin{cases} T_t - T_{base} \; if \; T_t > T_{base} \\ 0 \; otherwise \end{cases} \tag{3}$$

Various econometric specifications have been tested in the literature (see Fazeli et al., 2016, for a comprehensive review) to estimate the relationship between energy demand and temperature level. These approaches can be summarized as follows: the first strand of the literature focuses on linear and non-linear parametric methods. As mentioned above, the historical method is to model a linear specification with heating degree days (HDD) and cooling degree days (CDD). Initially, these models used a single balance point temperature for heating and cooling (Mitchell, 1984). For example, U.S. studies have often used 65°F (18.3°C) as the equilibrium point (Considine, 2000; De Dear and Brager, 2001; Donovan and Fischer, 1976; Pardo and Valor, 2002; Thom, 1954), while global analyses have favored 18°C (Isaac and Van Vuuren, 2009; Labriet, 2013). However, other studies have explored different balance point temperatures to better capture variations in energy use, using iterative methods (Kissock et al., 2003; Rüth and Lin, 2006).

Non-linear models have been developed to consider the complexities of consumer behavior and heating system capacities. With these models the level of temperatures itself is used with non-linear transformation such as polynomials. For example, Henley and Peirson (1997) found a polynomial estimation to better fit data on electrical space heating compared to linear models. Asadoorian et al. (2008) and Gelegenis (2009) used log-linear formulations and polynomials to estimate temperature elasticity in electricity demand.

The second part of the literature uses a semi/non-parametric method, i.e. the relationship between energy demand and temperature is not set a priori, but is defined by the model. Early on, Engle et al. (1986) introduced a semi-parametric regression method that combines linear elements for income and energy prices with cubic and piecewise linear splines for weather variables, this allows flexible modeling of the temperature-energy demand relationship. Carcedo and Vicéns-Otero (2005) applied the Logistic Smooth Transition Regression (LSTR) model, which effectively captures the smooth response of electricity demand to temperature variations, but also provides a method for validating the temperature thresholds traditionally used. Bessec and Fouquau (2008) extended this method to analyze electricity demand in EU member states, proving that the relationship between energy demand and outside temperature is non-linear for each country in the study. Later, Hurn et al. (2016) also used LSTR modeling to asses the effects of deregulation in the electricity of market, controlling by the temperature variations.

Our econometric framework combines these two strands of the literature by introducing the new general heating weather indicator GWI_{q_t}, specific for one energy demand q_t. This indicator is defined as the vector of the optimal linear combination of the K heating days

variables $\text{HDV}_{\{q_t, w_t^k = w_{base}^k\}}$. Where for $\text{HDV}_{\{q_t, w_t^k = w_{base}^k\}}$ we have $k \in 1, \ldots, K$ and $t \in 1, \ldots, T$ with T the number of observations and K the number of weather variables, among temperature, wind, sunlight duration, rain and cloudiness.

Building on the standard definition of the (HDD) (2), we define a heating days variable ($\text{HDV}_{\{q_t, w_t = w_{base}^k\}}$) for one specific weather variable (w_t^k) and one energy demand q_t as:

$$HDV_{\{q_t, w_t^k = w_{base}^k\}} = \begin{cases} w_{base}^k - w_t^k \ if \ sign(\rho_{\{q_t, w_t^k\}}) * (w_t^k > w_{base}^k) \\ 0 \ otherwise \end{cases} \tag{4}$$

where w_{base}^k is the optimal threshold(s) extracted using K-means that capture the non-linear relationship between the energy demand (q_t) and the k-th weather variable w_t^k (see Figure 2). To define one $\text{HDV}_{\{q_t, w_t^k = w_{base}^k\}}$, it is necessary to introduce the sign from the correlation between the energy demand q_t and the weather indicator w_t^k. For example for the production of standard HDD (or here, HDV where w_t^k is the temperature), the correlation between the energy demand and the temperature is negative, i.e. that lower temperature induces an increase in demand. Thus, the variable is different from zero if $-(w_t^k > w_{base}^k)$, in other terms, if $(w_t^k < w_{base}^k)$. At the opposite, for the production of the wind HDV, the correlation between the energy demand and the wind is positive i.e. that stronger wind speed induces an increase in demand. Thus, the variable is different from zero if $(w_t^k > w_{base}^k)$. The literature, also highlights the role of the air-conditioning (see Mitchell, 1984). We enhance our GWI, to take also into account this cooling effect. With similar notation of (4), we defined the CDV as follows:

$$CDV_{\{q_t, w_t^k = w_{base}^k\}} = \begin{cases} w_t^k - w_{base}^k \ if \ sign(\rho_{\{q_t, w_t^k\}}) * (w_t^k > w_{base}^k) \\ 0 \ otherwise \end{cases} \tag{5}$$

It is important to emphasize that w_{base}^k in (4) can differ from w_{base}^k in (5). For example, there could be a different value $w_{base_2}^k$ for the HDV threshold where heating begins and another value $w_{base_1}^k$ for the CDV threshold where cooling starts.

The next subsections present the K-means procedure to define potential thresholds for one couple of q_t and w_t^k and then the LASSO penalization that selects the optimal linear combination of both HDV and CDV for one q_t.

3.2.1 Numbers of regimes and threshold extraction

In time series analysis, a regime refers to a specific phase or period during which the underlying behavior or dynamics of the system being studied remain relatively consistent. In our study, a regime represents a distinct state or behavior in the relationship between weather variables and energy demand. Regime-switching models are often used to capture transitions between different states in the data. In this section we broadly recall the main methods to detect regime switch in the applied literature and introduce clustering as an alternative tool to extract regime switching.

A first approach in the literature to define the energy demand response function to temperature is drawn upon Carcedo and Vicéns-Otero (2005) and Bessec and Fouquau (2008),

which employs a Smooth Transition AR (STAR) method based on a predetermined definition of the data generation function. However, a smooth method induces an a priori definition of a function that best describes the relation between the series. One can also use, a non-smooth methodology grounded in the method of multivariate Threshold Vector Autoregression (TVAR) from Lo and Zivot (2001), based on the Self-extracting AR (SETAR) modelling (Chan et al., 1985). However, estimating thresholds in this setup is prone to sensitivity towards outliers or noise present in the data, which can lead to potentially biased or inconsistent estimates. Incorrect specification of the number of thresholds may result in misspecified models that fail to accurately capture the genuine underlying dynamics of the data. Empirically, it is uncommon to define more than three regimes with the associated two thresholds in a TVAR modelling because it becomes computationally heavy: every time a regime is added it strongly increases the size of the grid search. Moreover, in this context of the relationship between climate and energy demand, imposing a predetermined number of regimes a priori may overlook the true complexity of the relationship and means relying directly on visual representation and the existing shape of the relationship.[16] This underscores the need for a thorough and flexible approach to the model specification that allows for the discovery of the most appropriate response functional form and the number of regimes to accurately characterize this relationship. To do so, our approach relies on unsupervised classification and in particular using time-series clustering methods.

More formally, our time-series clustering can be defined as follows: given our dataset of a vector of two time-series containing q_t, and one of the n weather variables denoted by w_t^k. We define $D = \left\{q_t, w_t^k\right\}$, and we find an unsupervised partitioning of D into $C = \{C_1, C_2, \ldots, C_N\}$, where N is a hyperparameter correspond to the number of clusters that you need to set a priori. We make this partitioning in such a way that homogeneous time series are grouped based on a certain similarity measure (See Liao, 2005; Aghabozorgi et al., 2015, for a comprehensive review on the definition and application of clustering with time series.) [17]

Drawing on the seminal K-means algorithm (MacQueen, 1967), we operate iteratively assigning each data point to the nearest cluster centroid based on the Euclidean distance metric. Subsequently, the centroids are recalculated as the mean of the data points assigned to each cluster. This iterative process continues until convergence, resulting in clusters that exhibit similar characteristics or behaviors (see Algorithm 1).

[16] In appendix B.3, we perform a robustness analysis using the TVAR methodology. We find our approach is robust at the French national level, extracting similar thresholds. However, moving to the desegregated demand by regions, the heterogeneity of climate leads to the apparition of a cooling behavior and thus, for a constant number of regimes, the extracted threshold using the TVAR methodology is biased.

[17] Our application of clustering on time-series is similar to the Market Regime Clustering Problem (MRPC) in Finance (Horvath et al., 2021), MRPC involves segmenting returns into different groups or regimes, each characterized by distinct underlying distributions. Another close methodology is used by Greevy et al. (2024) to detect regime switching in finance time-series, but the clustering algorithm is used on statistics distribution variables rather than the series themselves.

Algorithm 1: k-means algorithm

Data: Set of T data points $D = \{q_t, w_t^k\}$ in $\mathbb{R}^2$, number of clusters N
Result: N clusters $C = \{C_1, C_2, \ldots, C_N\}$

Initialization: Choose N initial cluster centroids randomly: $C = \{c_1, c_2, \ldots, c_N\}$;
repeat
  for each data point $d_t = (q_t, w_t^k)$ **do**
    Assign d_t to the nearest cluster centroid:

$$\text{argmin}_{c_j \in C} \|d_t - c_j\|^2$$

  end
  Recalculate the cluster centroids as the mean of the data points assigned to each cluster;
  for each cluster C_j **do**
    $c_j = \frac{1}{|S_j|} \sum_{d_t \in S_j} d_t$ where S_j is the set of data points assigned to cluster C_j;
  end
until convergence;

One challenge in using the K-means algorithm is the requirement to pre-assign the hyper-parameters, the N number of clusters, which may not always be readily available or feasible to determine in real-world applications. This limitation can lower the algorithm's ability to produce natural clustering results and is recognized as one of its drawbacks. However, a potential solution, particularly when the data dimensionality is low, is to use the Standard Deviation Index. This index proposed by Halkidi et al. (2000) provides a robust validity measure that effectively balances compactness and separation. Their experimental study demonstrates that the SD index achieves the best trade-off between these two key criteria, making it a reliable choice for evaluating and selecting optimal clustering schemes.

Given clusters $C_1, C_2, \ldots, C_k$ with respective average intra-cluster variance $\sigma_1, \sigma_2, \ldots, \sigma_k$, the standard deviation index can be defined as:

$$\text{SD} = \alpha(\frac{1}{N} \sum_{k=1}^{N} \frac{\sigma_k}{\sigma}) + \min d(C_k, C_i)$$

The goal is to minimize the index as a lower value indicates clusters that are more compact and well-separated, which is desired in clustering tasks for ensuring clear and meaningful group differentiation.

3.2.2 Penalization procedure to construct the GWI

Once the pool of all the K weather variable-related HVD and CDV indicators is constructed, a variable selection process is employed through penalization. Penalization models incorporate a hyperparameter denoted as λ within the error term minimization process, to select the optimal linear combination among the regressors.

$$\begin{cases} q_t = \beta' X_t + \varepsilon_t \\ \min \sum^t (q_t - \hat{q}_t)^2 + \lambda ||\beta||_k \end{cases} \tag{6}$$

Where q_t, is one energy demand variable of T observations, $\beta = [\beta_1, \cdots, \beta_{2*K}]$ is $2 * K \times 1$ vector of the estimated coefficient of our linear penalization regression, and $X_t = \left[HVD_{q_t, w_t^1 = w_{base}^1}, \cdots, HVD_{q_t, w_t^K = w_{base}^K}, CVD_{q_t, w_t^1 = w_{base}^1}, \cdots, CVD_{q_t, w_t^K = w_{base}^K}\right]$ is a $2 * K \times T$ regressor weather vector, containing the HDV and the CDV.[18] ε_t is the residuals vector following a $N(0, \sigma^2)$, where σ^2 is variance matrix of the residuals.

The penalization model can be described as in equation (6) with λ the level of penalization, the higher $\hat{\lambda}$ the more penalized the model, the lower the $\hat{\lambda}$ the less penalized the model. $||\beta||_k$ reflects the norm, which is defined as the LASSO (l_1) norm in our approach, q_t denotes the initial seasonal time series and HDV_t is the weather indicator.[19] For robustness purposes, at each iterative step, we run 100 batches of estimation by varying the λ value in a range between 0.001 and 1 to test different levels of penalty. Then the mean of the 100 estimations is computed for each variable of the initial pool.

Denoted the optimal sparse penalized β^*, containing some zeros for the weather variables that are not selected by the LASSO procedure, we defined the GWI_{q_t} as:

$$GWI_{q_t} = \left[1_{\beta_1^* \neq 0} HVD_{q_t, w_t^1 = w_{base}^1}, \cdots, 1_{\beta_K^* \neq 0} HVD_{q_t, w_t^K = w_{base}^K}, 1_{\beta_1^* \neq 0} CVD_{q_t, w_t^1 = w_{base}^1}, \cdots, 1_{\beta_K^* \neq 0} CVD_{q_t, w_t^K = w_{base}^K}\right] \tag{7}$$

where $1_{\beta_k^* \neq 0}$, is a dummies variable taking the value 1, if the corresponding $HVD_{q_t, w_t^k = w_{base}^k}$ is selected and 0 if is not.

4 Empirical results

The goal of this paper is to develop a robust time series adjustment framework to facilitate accurate monitoring of the impact of national policies aimed at reducing energy consumption. Our primary application focuses on the analysis of a monthly database from January 2012 to December 2022. This extensive dataset allows us to study the general behavior of energy demand in relation to weather variations over a ten-year period.

4.1 A country specific base temperature

To illustrate how our proposed K-means-based approach estimates the optimal w_{base} for an HDV_{q_t} variable with respect to a demand q_t, we first examine the relationship between

[18] It is also possible to include all interaction terms between different HDVs (or CDVs). In our empirical illustration, none of these terms is selected, so we choose not to mention this in the methodology section for the sake of clarity.

[19] An argument could be made for using Ridge penalization instead of LASSO. However, LASSO was selected for variable selection because it excludes less relevant variables by shrinking their coefficients to zero. This approach enhances model interpretability and aligns with our goal of selecting only the most significant predictors, unlike Ridge regression, which retains all variables in the model by applying an l_2 norm.

the sectoral energy demands and the temperature variable. Figure 2 shows the relationship between ordered sectoral energy demand and ordered temperature, for natural gas and electricity. In this figure, the different dashed lines represent the extracted base thresholds w_{base} reported in the first column of Table 4 - Step 1, and the different colours represent the regimes defined by the clustering algorithm.[20] For temperature, Table 4 - Step 1 showcase two thresholds that represent base temperatures associated with distinct behavioral shifts in energy demand—one for moderate temperature changes and another for extremely cold conditions. This dual threshold was not at first expected but has already been suggested by Dubin (2008) relying on household panel data.[21] This result provides a more nuanced view of temperature-sensitive demand, which can inform public policies targeting energy efficiency and resource allocation under different weather conditions. Table 4 - Step 2, shows the value for the HDV related to temperature threshold is on average 15°C which is different from the thresholds that are commonly used in France for official statistics adjustment (17°C), the most commonly used in the literature (18°), or the recommended one by Eurostat. We define $HDV_{temp=EU}$ for further analysis developed in the rest of the paper, as the one recommended by Eurostat, and constructed as:

$$HDV_{temp=EU} = \begin{cases} T_{18} - T_t \; if \; T_t < T_{15} \\ 0 \; otherwise \end{cases} \tag{8}$$

Table 4: General Weather Indicator - Monthly

Step 1					
	Temperature	**Wind**	**Sunlight**	**Rain**	**Cloudiness**
$q_t^{Low_g}$	9; 15	3.5	378	2; 3	23; 24; 28
$q_t^{High_g}$	14	3.5	378	2; 3	23; 25; 28
$q_t^{Low_e}$	9; 15	3.5	378	2; 3	23.5; 24; 28
$q_t^{Med_e}$	10; 15	3; 3.5; 4	363	2; 2.5; 4	23; 24; 28
$q_t^{High_e}$	12; 13; 22	3; 3.5; 4	275; 300; 623	2;3	22, 24
Step 2					
	Temperature	**Wind**	**Sunlight**	**Rain**	**Cloudiness**
$q_t^{Low_g}$	15	-	378	-	-
$q_t^{High_g}$	14	-	378	-	-
$q_t^{Low_e}$	15	-	378	-	-
$q_t^{Med_e}$	15	3	363	-	-
$q_t^{High_e}$	13	3;4	-	2;3	-

Notes: Monthly energy consumption and weather data span the period from January 2012 to December 2022.

4.2 The role of weather variables beyond temperature

To highlight the role of the other weather variable, we estimate different w_{base} for all listed weather variables (w_t) in our dataset (see section 2 for the full list) using the GWI procedure

[20] For details regarding selecting the initial number of centroïd, please refer to appendix A.5.

[21] Please refer to appendix A.6 for a theoretical visual representation of a functional form with two thresholds.

Figure 2: Clustering analysis of monthly energy response to temperature

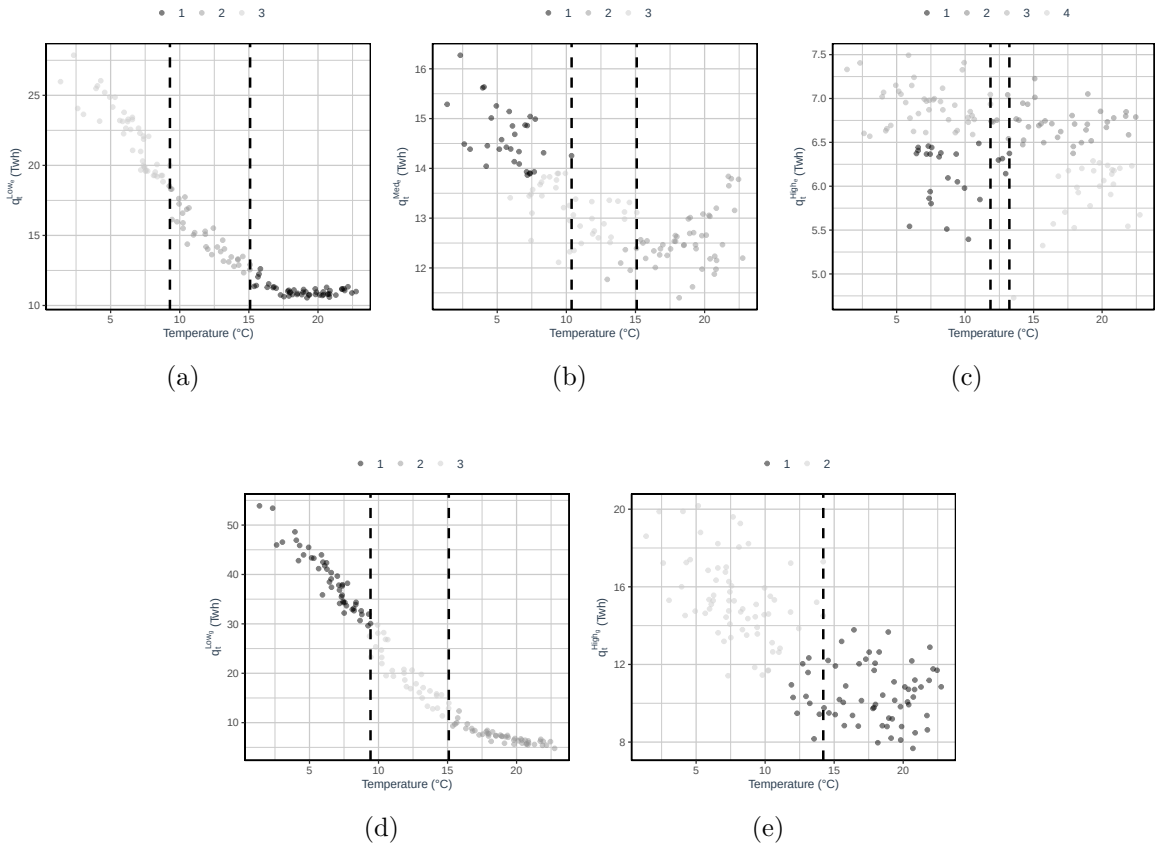

Notes : (a) $q_t^{Low_e}$ (b) $q_t^{Med_e}$ (c) $q_t^{High_e}$ (d) $q_t^{Low_g}$ (e) $q_t^{High_g}$. These figures are a visual representation of the K-means algorithm results. The dashed lines represent the regime-switching point, or base temperature and the clusters represent the different regimes. Monthly energy demand and weather data span the period from January 2012 to December 2022.

from section 3. Table 4 - Step 1 shows the estimated threshold for all considered variables, i.e. cloudiness, rain, sunlight and wind speed.[22] Then, our penalty selection procedure allows to define the GWI_{q_t} that is primarily composed of temperature, wind speed and sunlight duration, see Table 4 - Step 2. After constructing the GWI_{q_t} for each q_t, we analyze the output of the seasonal adjustment process with four different weather indicators : the full GWI that is denoted by $HDV_{temp=GWI}$, the optimal temperature from GWI denoted $HDV_{temp=15}$ and two benchmarks namely we consider $HDV_{temp=18}$, and $HDV_{temp=EU}$.[23]

In Table 5, we compare the four adjustment specifications, in order to showcase that the optimal specification is represented by the GWI. This table presents key metrics, including adjusted R^2 (R_a^2), Akaike Information Criterion (AIC), Root Mean Square Error (RMSE), and the p-value of the Ljung-Box test over the residuals ($p.value_{Q_{(1)}}$) to test the autocorrelation

[22]Figures showing the relationship between the ordered energy demand and the considered weather variable are available in Appendix A.4

[23]For simplicity, the different specifications are be reported as : GWI; 15; 18; EU in tables or figures.

and the squared the residuals ($p.value_{Q_{(2)}}$) to test the presence of heteroscedasticity. Additionally, we include the p-value of a Diebold and Mariano (1995)'s test ($p.value_{DM}(18|GWI)$) to statistically assess predictive accuracy .The choice of these metrics serves two main purposes: first, the AIC and Ljung-Box test ensure the selection of the best specification in terms of fitting the data. Consistent with Cui et al. (2023), the AIC is identified as the most effective criterion when working with weather-related data. Second, the RMSE and the Diebold-Mariano test focus on forecast-oriented performance. The Diebold-Mariano test plays a critical role in comparing predictive performances. Here, the null hypothesis assumes that the two models have equal predictive accuracy, while the alternative hypothesis suggests that the predictive performance of the GWI-based model is superior. Specifically, the test evaluates whether the average loss using $HDV_{temp=18}$ is greater than using $HDV_{temp=GWI}$ as weather control variable. Results from the test allow us to reject the null hypothesis, indicating that the GWI specification offers better predictive accuracy compared to the traditional HDD approach using 18°C as the base temperature. Furthermore, across all metrics, the GWI specification consistently emerges as the most optimal model. This is evidenced by its lower AIC and RMSE values, along with improved residual diagnostics that reduce autocorrelation, increase the independence of residuals, and produce a distribution more centered around zero. The Ljung-Box tests further confirms the independence of residuals, for the GWI specification, and suggests an absence of detectable autocorrelation and conditional heteroscedasticity, in contrast to the traditional HDD approaches.

Figure 3 and 4 showcase a top and a bottom panel, top panels display the adjusted time-series for the four different specifications and the bottom panels display the residuals distributions. These figures further support that the GWI, by including a more comprehensive set of weather variables, aims to capture more variability in energy consumption, as it reflects a broader spectrum of weather impacts that influence seasonal energy needs. Bottom panels further supports the effectiveness of the GWI by exhibiting a more concentrated distribution around zero, indicating a lower residual variance. This tighter fit implies that the GWI more accurately aligns with observed demand patterns, reducing the unexplained variance relative to the other specifications. The autocorrelation plot shows that the GWI method achieves lower residual autocorrelation across time periods compared to the HDD-based approaches. This suggests that GWI is more robust and effectively captures temporal dynamics in energy demand.

Table 5: Key metrics to highlight the optimal specification

	$q_t^{Low_g}$	$q_t^{High_g}$	$q_t^{Low_e}$	$q_t^{Med_e}$	$q_t^{High_e}$
$R_a^2(18)$	0.9949	0.9157	0.9927	0.9573	0.9145
R_a^2(EU)	0.9949	0.9172	0.9929	0.9585	0.9168
$R_a^2(15)$	0.9966	0.9253	0.9949	0.9604	0.9185
R_a^2(GWI)	0.9968	0.9341	0.9951	0.9691	0.9162
AIC(18)	374	355	176	14	-96
AIC(EU)	376	355	175	11	-99
AIC(15)	329	343	132	4	-102
AIC(GWI)	322	339	127	-19	-97
RMSE(18)	1.0561	0.9214	0.4443	0.2252	0.1463
RMSE(EU)	1.0601	0.9131	0.4371	0.2220	0.1443
RMSE(15)	0.8666	0.8673	0.3722	0.2167	0.1429
RMSE(GWI)	0.8353	0.8187	0.3636	0.1901	0.1442
$p.value_{Q_{(1)}}(18)$	0.0911	0.8771	0.9671	0.3087	0.4593
$p.value_{Q_{(1)}}$(EU)	0.1539	0.8179	0.9832	0.3114	0.5022
$p.value_{Q_{(1)}}(15)$	0.2903	0.9316	0.9821	0.8469	0.4760
$p.value_{Q_{(1)}}$(GWI)	0.2588	0.9725	0.9883	0.9681	0.8453
$p.value_{Q_{(2)}}(18)$	0.9881	0.8488	0.9164	0.0905	0.0815
$p.value_{Q_{(2)}}$(EU)	0.9722	0.8959	0.8267	0.0500	0.0896
$p.value_{Q_{(2)}}(15)$	0.9667	0.8914	0.6383	0.3066	0.1339
$p.value_{Q_{(2)}}$(GWI)	0.9615	0.9677	0.5248	0.8562	0.5245
$p.value_{DM}(18\|15)$	0.0012	0.0043	0.0004	0.177	0.0382
$p.value_{DM}(18\|GWI)$	0.0002	0.0016	0.0001	0.0018	0.1286
N	132	132	132	132	132

Notes: The table showcases results for five different metrics namely the adjusted R^2 (R_a^2), Akaike Information Criterion (AIC), Root Mean Square Error (RMSE), the p-value of the Ljung-Box test ($p.value_Q$),and the p-value for Diebold-Mariano tests ($p.value_{DM}$). The analysis uses monthly energy consumption and weather data spanning the period from January 2012 to December 2022.

Figure 3: Seasonal adjustment and residuals distributions for q_t^g

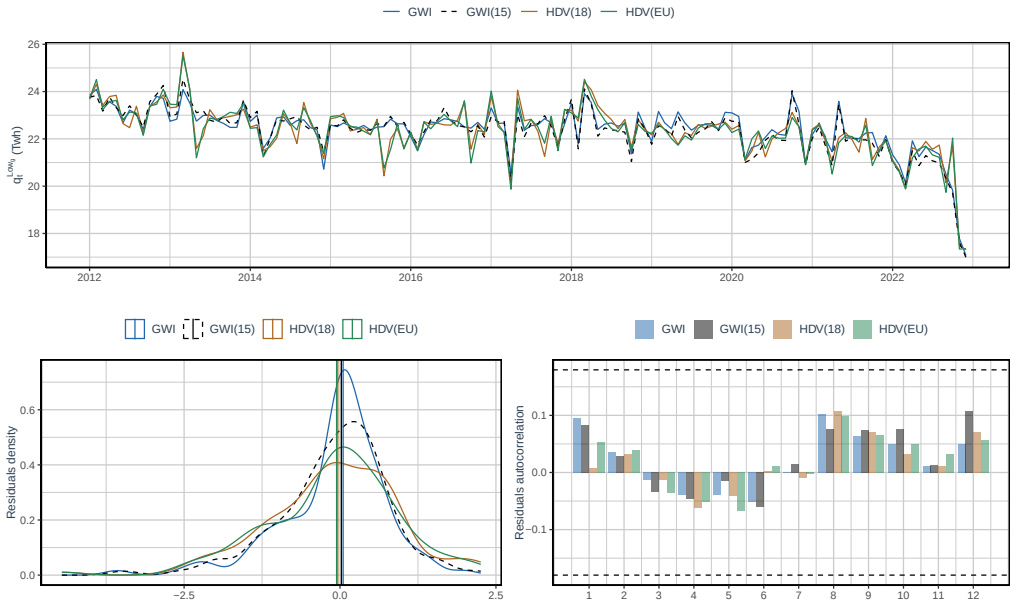

(a)

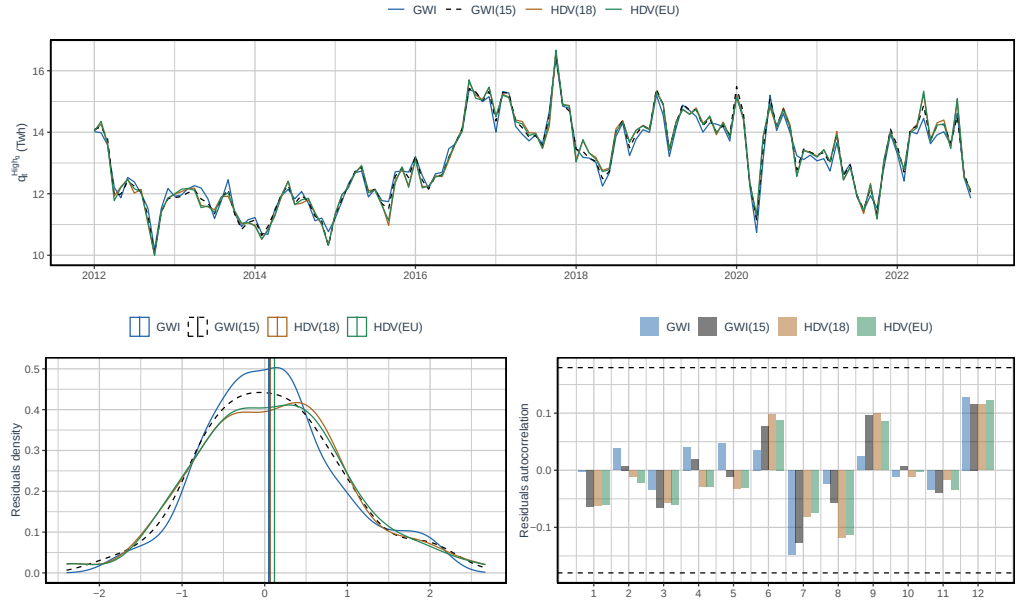

(b)

Notes : The figure displays seasonal adjustment and residual distributions for (a) $q_t^{Low_g}$ (b) $q_t^{Med_g}$. The top panel shows the seasonally adjusted time-series for four specifications. The bottom panels illustrate the residual distributions, with the left panel showing residual density and the right panel presenting residual autocorrelation by month.

Figure 4: Seasonal adjustment and residuals distributions for q_t^e

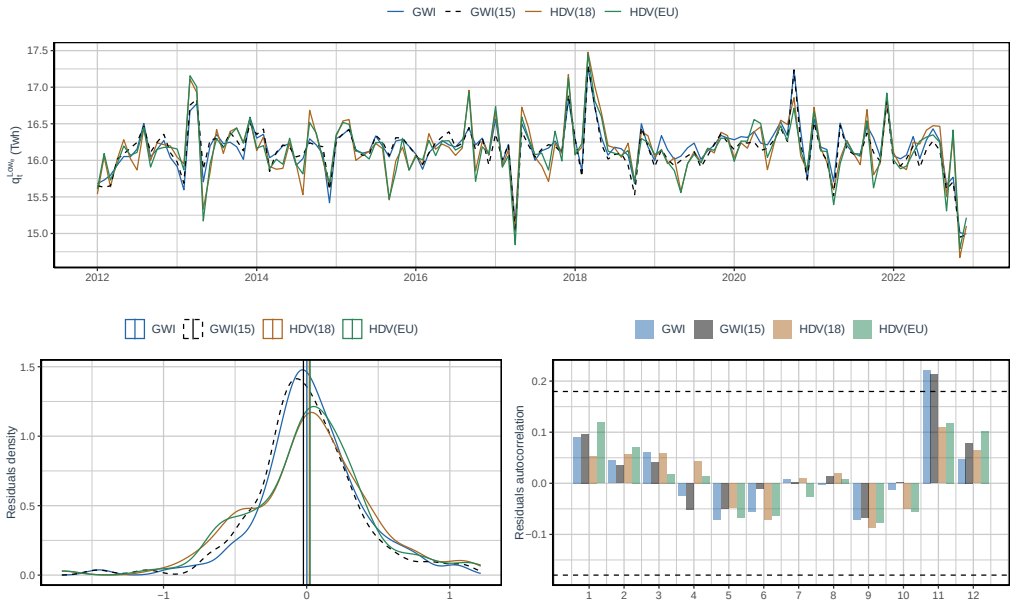

(a)

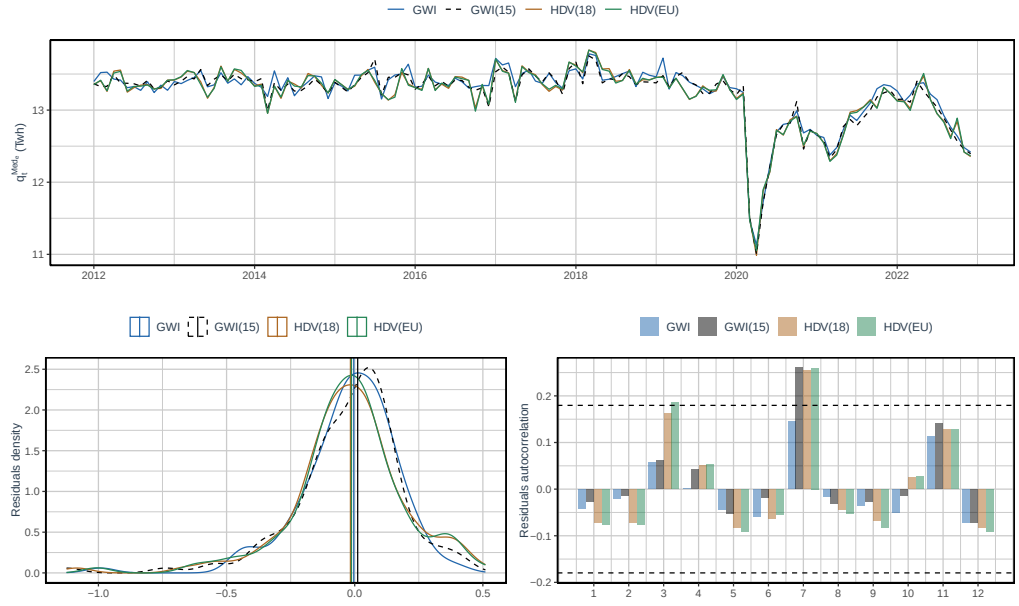

(b)

Notes : The figure displays seasonal adjustment and residual distributions for (a) $q_t^{Low_e}$ (b) $q_t^{Med_e}$. The top panel shows the seasonally adjusted time-series for four specifications. The bottom panels illustrate the residual distributions, with the left panel showing residual density and the right panel presenting residual autocorrelation by month.

4.3 Economic implications

This section presents two principal economic implications of the empirical results. Firstly, the shape of the relationship between energy demand and weather variables is analyzed. This contributes to a body of literature that characterizes consumer behavior in response to weather variations across a year (see for exemple Engle et al., 1986; Dubin, 2008). This provides insights into the need for heating and/or cooling, as well as the existence of a so-called comfort zone where energy use is not needed to regulate building temperature. We then discuss the impact of our approach on the estimated weather elasticity, which is crucial for policymakers and energy providers as it informs strategies for energy supply management and infrastructure planning (see for example Chaton, 2024; Giraudet et al., 2021; Thao Khamsing et al., 2016). By quantifying the manner in which energy demand responds to weather fluctuations, it facilitates the development of more accurate predictive models, which can be used to mitigate the effects of extreme weather events on energy systems (see Sgarlato and Ziel, 2023).

4.3.1 Functional form of France energy demand

To refers to the form of the relationship between temperature and energy demand, the literature relies on letters. The first form was describe by Jäger (1983) and define as a V-Shaped (see Figure 5-a) with a unique balance point between cooling and heating with thus no comfort zone. Then, the concept of comfort zone was introduced by Carcedo and Vicéns-Otero (2005) and the relationship then described as U-Shaped (see Figure 5-b). However, for specific country such as France, where the use of cooling device is not usual, the U-Shaped relationship becomes L-Shaped as the cooling behavior is not relevant anymore (see Figure 5-c). To go further, both U-Shaped and L-Shaped relationship exhibit a concept of "comfort zone", highlighted in red in Figure 5. This “comfort zone” refers to the range of temperatures within which economic agents experience no significant behavioral response to temperature variation. Within this range, individuals and organizations do not perceive the need to adjust their energy consumption to heat or cool their environment. In other words, energy demand remains relatively stable because conditions are naturally perceived as comfortable without additional intervention (Eskeland and Mideksa, 2010; Hekkenberg et al., 2009; Carcedo and Vicéns-Otero, 2005). Based on the literature, the usual boundaries for the comfort zone are temperatures below 18°C, where heating becomes necessary, and above 21°C, where cooling becomes relevant.

In this context, our study aims to define the functional form for France based on empirical evidence and to redefine the comfort zone boundaries. Similar to the estimates presented in Table 6, Figure 6 illustrates the two main empirical functional forms for France. The first represents an L-shaped function with a single balance point at 15°C, marking the transition between the heating zone and the comfort zone. The second represents a V-shaped function, observed only in electricity demand from the tertiary sector, again with a single balance point marking the transition between the heating and cooling zones. This V-shaped function suggests that there is no significant comfort zone and that economic agents, on average, switch directly from heating to cooling in the tertiary sector.

Figure 5: Functional form from the literature

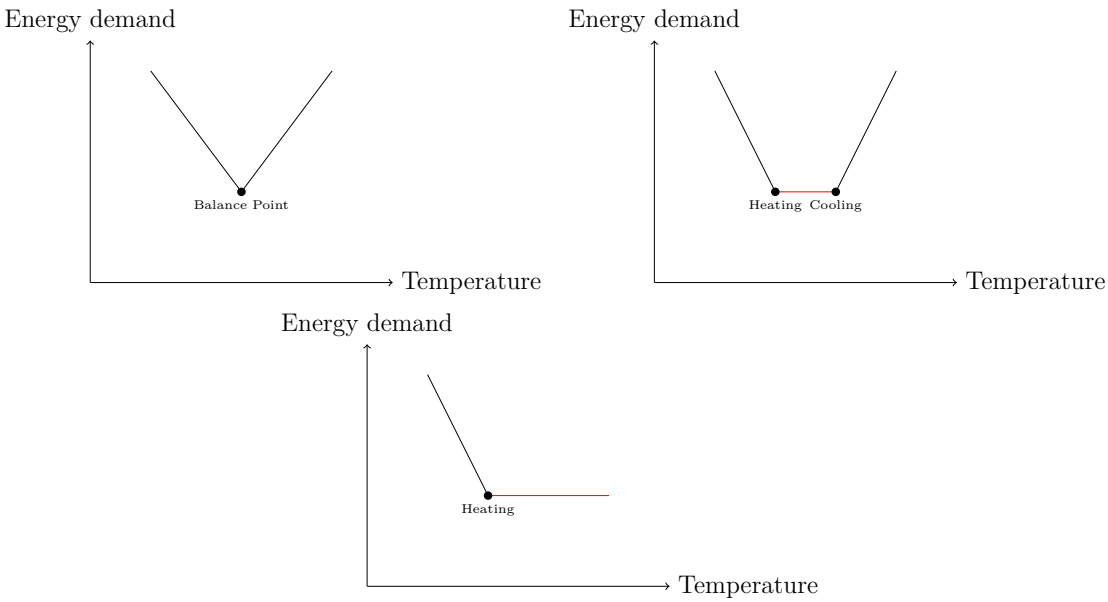

Notes : (a) V-shaped - (b) U-shaped - (c) L-Shaped

Figure 6: Functional form from empirical evidences - Temperature

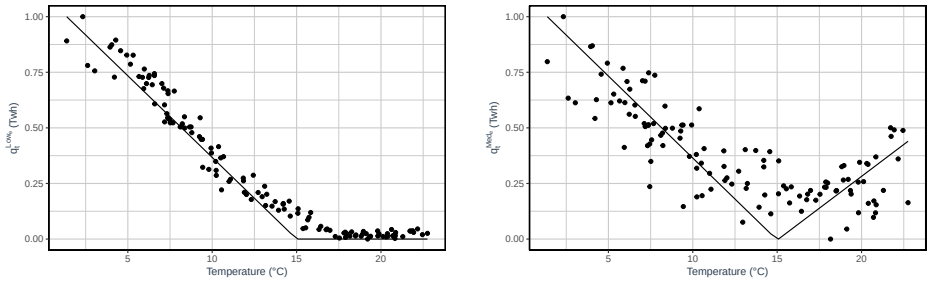

(a) (b)

Notes : (a) $q_t^{Low_e}$ (b) $q_t^{Med_e}$

Beyond temperature, however, energy demand is also influenced by other environmental variables, such as wind speed and sunlight, which contribute to the broader concept of "felt temperature." This concept reflects how individuals perceive environmental conditions based not only on temperature but also on additional factors that affect thermal comfort. As demonstrated in Figure 7, wind speed (Figure 7-b) exhibits a positive correlation with energy demand, as higher wind speeds increase heat loss and create a greater need for heating. Similarly, sunlight (Figure 7-a) inversely affects energy demand, as increased solar radiation reduces heating requirements by naturally warming indoor and outdoor spaces. These findings suggest that models of energy demand should incorporate these additional variables to

account for their impact on perceived thermal comfort, thereby providing a more nuanced understanding of the determinants of energy demand.

Figure 7: Functional form from empirical evidences - Beyond temperature

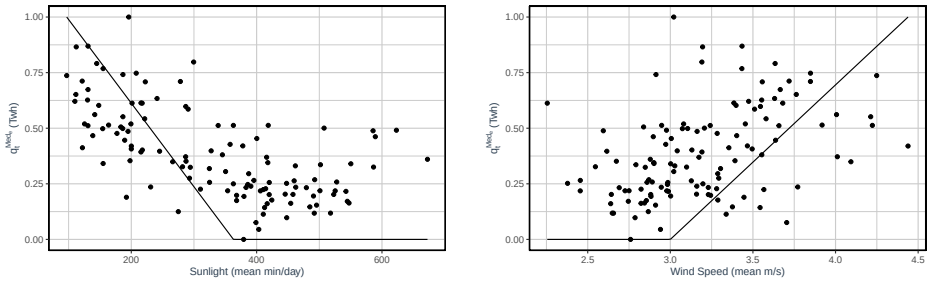

(a) (b)

Notes : (a) Sunlight (b) Wind Speed

4.3.2 Weather elasticities estimate

The coefficients reported in Table 6 represent the thermosensitivity estimates expressed in TWh/HDV (resp. TWh/CDV) that can be interpreted as the increase of energy demand in TWH when the HDV (resp. CDV) increase of 1°C, *ceteris paribus*. For example, if there were one extra heating degree-day per day for an entire month, residential electricity consumption ($q_t^{Low_e}$) would rise up to 1.014 TWh (0.0338*30 = 1.014, see Table 5). Additionally, the specification incorporates the estimation of the COVID-19 effect $D_{03-2020}$, the estimated coefficient is both significant and negative, except for residential electricity demand. This result aligns with expectations, as confinement policies increased residential energy consumption while reducing demand in other sectors due to economic slowdowns and reduced industrial activity.

The thermosensitivity coefficients provide valuable insights into sector-specific weather elasticities. These results underscore the importance of sector-specific analyses of weather elasticities in energy demand. Indeed, the residential sector emerges as the most thermosensitive, as a significant share of its energy consumption is dedicated to heating. According to the GWI specification, thermosensitivity in this sector is reflected in higher coefficients across all quantiles compared to other sectors, demonstrating a pronounced responsiveness to weather variations. Electricity demand in the residential sector exhibits a relatively lower thermosensitivity than heating-related energy sources, as electricity is also used extensively for non-heating purposes such as powering household appliances. In contrast, the tertiary sector shows lower overall thermosensitivity CGDD (2023). While the coefficients for heating-related energy sources such as natural gas or district heating are comparable to the residential sector, the electricity demand in this sector is less responsive to weather changes. This is consistent with the dominance of non-heating uses of electricity, including lighting, office equipment, and other specific applications. These sector-specific results highlight the effectiveness of the GWI approach in capturing thermosensitivity patterns and point to its

potential for disaggregated analyses.

Table 6: Monthly estimates of Thermosensitivity (TWh/HDV)

	$q_t^{Low_g}$	$q_t^{High_g}$	$q_t^{Low_e}$	$q_t^{Med_e}$	$q_t^{High_e}$
$HDV_{temp=GWI}$	0.0928***	0.0230***	0.0338***	0.0086***	0.0023**
	(0.0020)	(0.0020)	(0.0009)	(0.0005)	(0.0003)
$CDV_{temp=GWI}$				0.0064**	
				(0.0008)	
$D_{03-2020}$	-1.6702*	-2.2721*	0.1710	-1.8622**	-0.8645**
	(0.6566)	(0.9600)	(0.2807)	(0.2034)	(0.1417)
N	132	132	132	132	132

Notes: The estimates are derived from a regSARIMA model, with monthly energy consumption levels (in TWh) as the dependent variable. The table presents estimates for temperature components that significantly impact energy consumption and the Standard errors associated with each coefficient are provided in brackets. Each regression incorporates fixed SARIMA components to capture cyclic patterns, as well as fixed control variables for business days, the COVID period, leap years, weekends, and holiday effects. For the SARIMA component, the polynomial orders δ, Φ, and Θ are determined and fixed based on the Autocorrelation Function (ACF) and Partial Autocorrelation Function (PACF). As a result, the process is defined as $(1,0,1)(0,1,1)$. The analysis uses monthly energy consumption and weather data spanning the period from January 2012 to December 2022.

We now focus on thermosensitivity in the industrial sector. First, it is important to note that industrial gas consumption behaves differently from electricity consumption because it includes gas-fired power plants that support electricity supply during periods of low temperatures, thereby inducing stronger thermosensitivity with a coefficient estimated at 0.023 TWh/HDV, in contrast to electricity, which has a coefficient of 0.002 TWh/HDV.[24] Focusing on electricity consumption $q_t^{High_e}$ in the industrial sector, while we suspect no significant relationship with weather variations, we still apply our methodology to this time-series. As Figure 8 and Table 5 illustrate, our approach reveals a minimal yet measurable thermosensitivity in the industrial sector with respect to temperature variations. Specifically, our approach proves suitable as the statistical significance of the coefficient estimated from the GWI highlights that weather conditions play a minor but significant role. This finding underscores the weak dependence of industrial electricity consumption on temperature changes, consistent with expectations given the lower heating and cooling requirements in this sector. The analysis of the different metrics demonstrates that while thermosensitivity is small, it remains relevant to use the optimal weather regressors, as the residuals' distribution and autocorrelation are well-behaved. This demonstrates the robustness of our methodology even in contexts where weather-induced energy demand variations are expected to be limited.

To compare our estimates with those found in the literature, we present the estimated sectoral thermosensitivity in different ways. Specifically, Considine (2000) reports semi-elasticities, which are interpreted as the percent change in aggregate energy consumption for a one-degree day deviation per day. Table 7 presents our estimates of these semi-elasticities, interpreted as folow: if there were one additional heating degree day per day over an entire month, residential electricity consumption would increase by 0.54% ($0.018 \times 30 = 0.54$).

[24]Please note that here the variable GWI represents a heating degree variable with a base temperature defined at 13°C, as presented in Table 4. For consistency with the other time-series, we still compare it to our benchmark and the country-specific base temperature of 15°C as defined previously.

Figure 8: Seasonal adjustment and residuals distributions for $q_t^{High_e}$

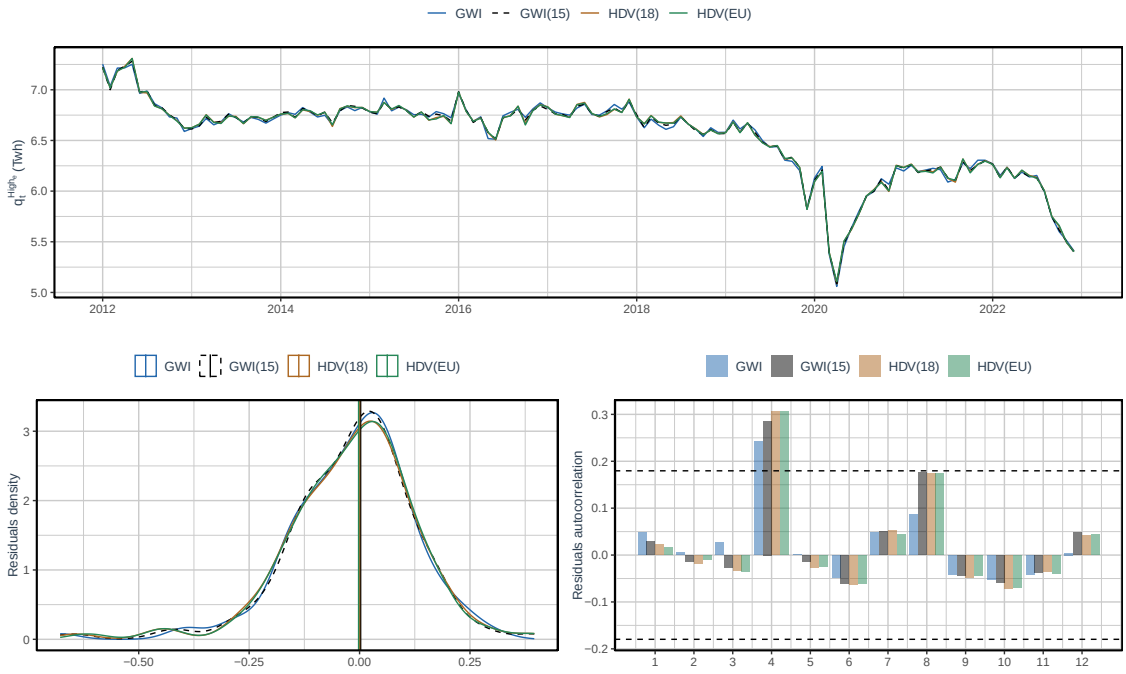

Notes : The figure displays seasonal adjustment and residual distributions for $q_t^{High_e}$. The top panel shows the seasonally adjusted time-series for four specifications. The bottom panels illustrate the residual distributions, with the left panel showing residual density and the right panel presenting residual autocorrelation by month.

For residential electricity demand, our estimated semi-elasticity is 0.018%, which closely aligns with the values reported by Considine (2000), ranging from 0.016% to 0.018%. For gas demand, our combined residential and tertiary sector estimate of 0.035% is consistent with the broader findings in the literature, which suggest that gas demand elasticities tend to be higher than those for electricity, particularly in the residential sector. Finally, the industrial gas demand elasticity in our study is 0.015%, which is slightly higher than the 0.013% reported by Considine (2000). Second, we also estimated that approximately 26% of residential electricity use is dedicated to heating, as shown in Table 7.[25] This estimate aligns closely with the 27% reported by *Electricité de France* (EdF), the main electricity producer in France (EdF, 2024). This consistency between our findings and EdF's estimates supports the robustness of our approach in quantifying the share of electricity used for heating.

[25]The thermosensitivity share is calculated as follows: the thermo-sensitivity estimate is multiplied by the annual HDV, yielding the consumption level attributed to heating purposes. This value is then divided by the annual total consumption, allowing the thermosensitivity share to be derived.

Table 7: Thermosensitivity as shares and semi-elasticities

	Average Annual Consumption (TWh)	
	Gas	Electricity
Residential	263	192
Tertiary		158
Industrial	155	78
	Thermosensitivity as semi-elasticities (%)	
	Gas	Electricity
Residential	0.035%	0.018%
Tertiary		0.005%
Industrial	0.015%	0.003%
	Average Thermosensitivity Share (%)	
	Gas	Electricity
Residential	53%	26%
Tertiary		8%
Industrial	22%	4%

Notes : The semi-elasticities are approximated by calculating the ratio between the thermosensitivity coefficient (in levels) and the average consumption. The thermosensitivity share is derived as the proportion of total consumption attributable to heating purposes. This is calculated by multiplying the thermosensitivity coefficient by the annual average number of heating degree days (1495), and dividing the result by the total annual average consumption.

5 Robustness analysis

This section provides a robust analysis of our GWI approach to, time subsample, daily and spatial data, considering 12 administrative regions of France.[26]

5.1 Rolling time window analysis

This section aims to test the robustness of the GWI over time, comparing it to the two standard HDD benchmarks. We focus solely on the temperature-related HDV and $q_t^{Low_e}$, as other weather variables were neglected in the previous literature. We demonstrate that the base temperature indeed changes over time, which is the first criticism of the standard HDD. Additionally, we show that the GWI selects the optimal value for the temperature HDV in any time sub-sample. Recall that Section 4.1 presents an application using monthly aggregated data from January 2012 to December 2022. In this section, we perform a rolling exercise using ten-year moving windows from 2000 to 2022, providing an overview of the variations in the optimal composition of the GWI_{q_t} index, shown here for $q_t^{Low_e}$.

Figure (9) illustrate the outcomes of the rolling LASSO exercise concerning the HDV_{temp} selection, initially the benchmarks and the country-specific temperature are proposed, namely: $HDV_{temp=18}$; $HDV_{temp=EU}$ and $HDV_{temp=15}$.

First, for each time step, the Eurostat double threshold is never selected. Second, the

[26]The 12 administrative regions considered are the metropolitan administrative regions, without *Corse* that is not served by ENEDIS for $q_t^{Low_e}$.

Figure 9: HDV_{temp} LASSO estimates on time-varying window

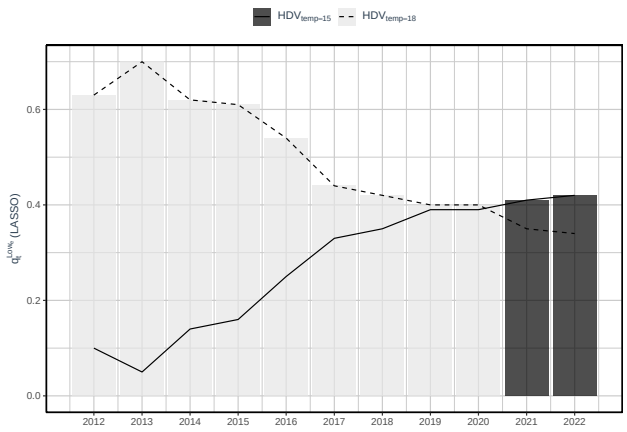

Notes : The figure displays the result of a rolling exercise, over the period 2000-2022, with a different ten years window at each rolling step. The lines represent the level of the coefficients estimated by LASSO and the bars represents the selected variable at each steps.

base temperature of 18°C, as defined in the literature, is initially the most commonly selected by the LASSO processes. However, over time, the estimated coefficient for a base temperature of 15°C is progressively less penalized, eventually surpassing that of 18°C. This result suggests that, in France, between 2000 and 2022, there has been a shift in behavior regarding the temperature at which agents begin heating their premises. While the base temperature is often assumed to be constant over time, despite potential changes in behavior or technology (Kennard et al., 2022), our proposed approach demonstrate that changes do occur, they are however relatively smooth and not frequent. Due to the design of this study, it is only possible to hypothesize on the determinants of this empirical change in behavior. Two main hypotheses emerge: on the one hand, improvements in the energy efficiency of the housing stock, particularly through thermal renovation, may have reduced the need for heating at higher temperatures. On the other hand, changes in habits, possibly linked to greater environmental awareness or policies aimed at reducing energy demand, such as energy sobriety initiatives, could also play an important role. This result emphasizes the need to tailor the threshold to the specific sub-sample being studied, as different time windows could result in different behavioral responses to temperature. This could raise concerns about the comparability of the policy evaluation across different time-varying subsamples. To illustrate, a substantial policy investment in energy-efficient buildings should result in a shift to a lower baseline temperature due to increased building insulation.

5.2 Daily data

To study the robustness of our approach to higher frequency, we apply the same procedure as in section 4 to the daily data, to decompose the optimal base temperature and possible other weather regressors. Recall that at the daily frequency, *only residential electricity demand*

is available. Applying our procedure to determine the daily GWI for low voltage electricity demand again leads to the definition of a base temperature of 15°C (see Table 8 and Figure 10). The non-linear relationship between energy demand and temperature is similar to that estimated using the monthly dataset as shown in Figure 2 -(a). However, in opposite to monthly data, Figure 10 shows a stronger variability in the demand level for a constant temperature, inducing significant effects from other sources than temperature such as the wind speed and the sunlight duration as selected in the GWI by our methodology.

Table 9 confirms that the optimal specification is the GWI with a base temperature at 15. It leads to the estimation with both the lowest AIC and RMSE. Morever the p-value of the Diebold-Mariano test asses that the model has better predictive power when specified with either only $HDV_{temp=15}$ or the whole GWI, compare to a HDD at 18. The thermosensitivity estimates is still expressed in TWh/HDV that can be interpreted as the increase of energy demand in TWH when the HDV increase of 1°C, ceteris paribus. The estimated coefficient is estimated at 0.0213 TWh/$HDV_{temp=GWI}$. This is lower than the estimate of 0.0338 TWh/$HDV_{temp=GWI}$ presented in Table 6. This difference can be explained by the variation in the time span of the data between the two samples: the main sample covers a ten-year period, while the second sample only includes data from 2019 to 2022, which contains exceptional years in terms of energy consumption. Specifically, 2020 and 2021 were influenced by the COVID-19 pandemic, while 2022 saw a significant decrease in consumption, -10.2%, due to multiple factors such as inflation and energy-saving policies (CGDD, 2023).

Figure 10: Clustering analysis of daily low tension electricity response to temperature

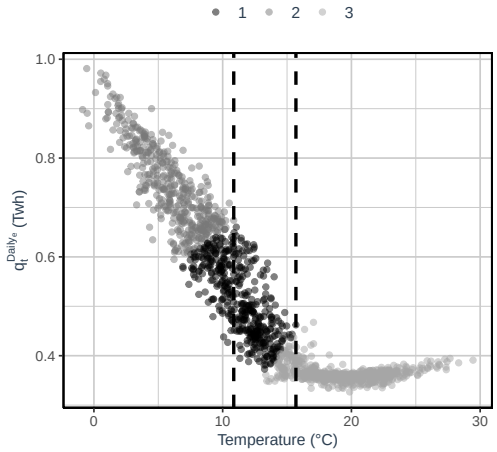

Notes : This figure is a visual representation of the K-means algorithm results for three different regimes. The vertical red line represents the regime-switching point, or base temperature, between the non-heating and heating periods. Daily electricity consumption spans the period from January 1, 2019, to December 31, 2022.

Table 8: General Weather Indicator - Daily

		Step 1		
	Temperature	**Wind**	**Sunlight**	**Rain**
$q_t^{Daily_e}$	9; 15	4.2; 4.5	500; 592	2.4; 2.9; 3.8; 6.6; 8.9
		Step 2		
	Temperature	**Wind**	**Sunlight**	**Rain**
$q_t^{Daily_e}$	15	4.5	500	-

Notes: Daily electricity consumption and weather data span the period from January 1, 2019, to December 31, 2022.

Table 9: Daily estimates of Thermosensitivity (TWh/HDV)

	$q_t^{Daily_e}$
$HDV_{temp=GWI}$	0.0213***
	(0.0030)
R_a^2(18)	0.9983
R_a^2(EU)	0.9980
R_a^2(15)	0.9991
R_a^2(GWI)	0.9992
AIC(18)	-2777
AIC(EU)	-2778
AIC(15)	-2825
AIC(GWI)	-2828
RMSE(18)	0.0072
RMSE(EU)	0.0078
RMSE(15)	0.0051
RMSE(GWI)	0.0049
$p.value_{DM}(18\|15)$	0.0000
$p.value_{DM}(18\|GWI)$	0.0000
N	730

Notes: The estimates are from regSARIMA with daily energy consumption level in TWh as the dependent variable. The table presents estimates for temperature components that significantly impact energy consumption. Additionally, the model includes estimates for other weather components under the GWI specification. Each regression also incorporates fixed SARIMA components, capturing cyclic patterns and fixed control variables for business days, leap years, weekends, and holiday effects. For the SARIMA component order of polynomials δ. Φ and Θ are fixed along the defined using the Autocorrelation Function (ACF) and Partial Autocorrelation Function (PACF) (see Figure 13 in Appendix A.3). Thus, the process is defined as (7.0.1)(0.1.1). Daily electricity consumption and weather data span the period from January 1, 2021, to December 31, 2022.

5.3 Regional data

This section used a daily disaggregated dataset for each of the 12 regions, to unravel the optimal weather vectors across France. We present the first step using the K-means procedure and it defines an average, normalized, base temperature of 15°C as reported in Table 10. However, the regional decomposition shows a non-continuity in the base temperature detected for each region. In particular, the region *Provence-Alpes-Côte d'Azur* shows a HDV_{temp} and CDV_{temp} related to the temperature effects, it leads to classify this region has having a U-shape functional form as describe in Section 4.3.1 meaning with a summer thermo-sensitivity linked to the use of cooling devices. Appendix B.2 shows the cluster detection in the case of *Provence-Alpes-Côte d'Azur* compare to another region.

Furthermore, Table 10 illustrates the baseline temperature using the clustering algorithm and the SETAR procedure. The results demonstrate that the K-means approach produces a

more robust estimate in the presence of spatial heterogeneity. The columns labelled *RMSE* show the root mean square error (RMSE) for the regSARIMA process using the two methods. The results demonstrate that the temperatures extracted by K-means led to a more optimal estimation than with SETAR. This indicates that clustering methods are more robust to spatial heterogeneity. However, both methods produce comparable results at the aggregate level (see Appendix B.3 for details).

Table 10: Estimated base temperature for regionals HDV

	$HDV_{temp}^{K-means}$			HDV_{temp}^{SETAR}		
	estimated	round	RMSE	estimated	round	RMSE
Grand Est	14.14	14	1.02	14.46	14	1.02
Normandie	14.45	14	2.02	12.93	13	2.20
Hauts-de-France	14.47	14	1.51	13.27	13	1.62
Bretagne	14.65	15	2.10	15.27	15	2.10
Centre-Val de Loire	14.72	15	1.90	12.86	13	2.23
Bourgogne-Franche-Comté	14.75	15	1.34	16.03	16	1.35
Auvergne-Rhône-Alpes	14.79	15	1.39	17.93	18	1.47
Pays de la Loire	15.47	15	2.04	16.80	17	1.93
Île-de-France	15.70	16	1.40	12.73	13	1.72
Occitanie	16.20	16	1.49	19.14	19	1.49
Provence-Alpes-Côte d'Azur	16.69	17	1.36	19.20	19	1.42
Nouvelle-Aquitaine	17.46	17	1.52	18.69	19	1.60
Mean	15.25	15	1.47	15.86	16	1.53
Weighted Mean	15.45	15	-	16.01	16	-

Notes : The base temperatures are defined using the K-means algorithm in a two-dimensional environment: energy consumption and temperature level. The lowest temperature of each regime is extracted and registered as the base temperature for regime switching. The table shows the base temperature for the regime switching between the non-heating and heating periods. The national weighted mean is computed using the number of households recorded in the French national census from 2020. Regional daily energy consumption spans the period from January 1, 2022, to December 31, 2022.

Table 11 presents the estimated weather coefficients with a regSARIMA specification. For clarity purposes, only the estimated coefficients are reported and if the estimate was not significant than it has been presented as "-". In terms of the level of the estimates, it represents the variation of demand in kWh per household for a variation of one unit from the different weather indicators. Table 11 is shorted according to the thermo-sensitive estimate level, from the lowest to the highest one. The strongest thermo-sensitivity coefficient is estimated for the region *Normandie* and the smallest for the region *Grand Est*, highlighting the heterogeneity in the estimated thermo-sensitivity. Thus, in *Normandie*, a deviation of one heating-degree day is estimated as resulting in an increase of 1.34 kWh in energy consumption per household. The last row of Table 11, showcase the estimated aggregate thermosensitivity coefficient, presented in TWh. This value is obtained in two steps: first, by multiplying the initial regional coefficients, expressed in kWh per household, by the number of households in each region. In the second step, each regional coefficient is converted into TWh, and then we average across all regions. The value obtained is 0.0405 (TWh/HDV). This differs from the 0.0338 (TWh/HDV) estimate obtained in section 4.1, without accounting for spatial heterogeneity, which reflect regional differences in heating habits.

Regarding the GWI, there is heterogeneity depending on the climate zone on which the

administrative region depends. First, the correlation table (see Table 20 in appendix A.3) shows that the temperature correlation is strong for all regions, but can be relatively smaller for regions from hot climatic zones, where there is probably a cooling degree effect. Then, the sunlight and wind correlations are on average lower than at the national level. The estimation on Table 11 can be interpreted in terms of GWI, the estimation allows us to develop our interpretation in terms of the pool of significant weather indicators for each region. First, we again identify the region with a significant cooling effect: *Provence-Alpes-Côte d'Azur*. This region is located in a hot climatic zone in the southern metropolitan area of France. Secondly, the effect of sunlight and wind speed are mostly significant as expected with a positive estimate, meaning that an increase in wind speed leads to an increase in demand and a decrease in sunlight duration also leads to a decrease in demand. Finally, for three regions, among the one *Bourgogne-France-Comté* which is the most rainy region in the last years, the rain amount plays a significant role.

Table 11: Regional daily estimates response to weather sensibility (kWh/Household/HDV)

	HDV_{temp}	CDV_{temp}	HDV_{wind}	$HDV_{sunlight}$	HDV_{rain}
Grand Est	0.6591	-	0.4671	0.0063	-
Île-de-France	0.8361	-	0.6305	0.0058	-
Bourgogne-Franche-Comté	0.8744	-	0.8408	0.0049	0.0601
Auvergne-Rhône-Alpes	0.9535	-	0.5333	-	-
Hauts-de-France	0.9776	-	0.4314	0.0185	-
Nouvelle-Aquitaine	1.0332	-	0.7309	-	0.0889
Occitanie	1.1622	-	-	-	-
Centre-Val de Loire	1.1700	-	0.7871	0.0099	-
Provence-Alpes-Côte d'Azur	1.1946	0.4625	0.3185	-	-
Pays de la Loire	1.2795	-	0.6188	0.0151	-
Bretagne	1.2900	-	0.5087	0.0177	-
Normandie	1.3372	-	0.6179	0.0168	0.1006
Mean (kWh/Household)	1.0639	0.0385	0.5404	0.0079	0.0208
Mean (TWh)	0.0405	0.0015	0.0206	0.0003	0.0008

Notes : The estimates are from a regSARIMA regression with regional daily energy demand levels in kWh/household as the dependent variable. For clarity, non-significant estimates have been reduced to 0. The table presents the estimates for weather components that significantly impact energy demand. The estimates for HDV_{temp} variables can be interpreted as the sensitivity to cold temperatures. The estimated coefficients for the HDV_{wind} variables represent sensitivity to strong wind speeds, $HDV_{sunlight}$ variables as sensitivity to lower sunlight duration, and HDV_{rain} variables as sensitivity to an increase in the millimeters of rain during a 24-hour period. Additionally, the model estimates the SARIMA components, i.e., the cyclic elements, and control variables for business days, leap years, weekends, and holiday effects. Regional daily energy demand spans the period from January 1, 2022, to December 31, 2022.

6 Conclusion

The use of standard HDD faces three main criticisms: the lack of statistical criteria to define the base temperature, the reliance solely on temperature as the weather variable, and the assumption of a constant base temperature over time and space. To address these concerns, this study introduces a statistically validated approach—the General Weather Indicator (GWI)—to analyze weather effects in energy consumption seasonal adjustment, with an application to France's electricity and natural gas consumption. Our statistical procedure relies on a clustering algorithm (K-means), followed by a LASSO penalization procedure. This indicator advances the understanding of temperature response functions and their underlying assumptions. First, our results challenge the conventional use of static base temperatures, such as 18°C for HDD (Heating Degree Days) and 21°C for CDD (Cooling Degree Days), by identifying dynamic base temperatures. Second, our analysis reveals the spatial variability of temperature sensitivity. Regional differences in energy demand responses highlight the significant limitations of assuming a uniform base temperature across diverse geographical regions. For example, while some regions exhibit typical L-shaped temperature-demand relationships, similar to the national scale, others display distinct patterns driven by specific behaviors, such as increased cooling demand during summer in parts of southeast France. These regional variations reflect local climatic conditions, building characteristics, and energy-use habits. Finally, we expand beyond temperature as the sole weather indicator by incorporating additional variables such as solar radiation and wind speed. The inclusion of these variables, supported by robust statistical validations, underscores their importance in refining energy demand models. For instance, incorporating solar radiation significantly enhances model performance, as evidenced by various metrics (*AIC, RMSE, adjusted* R^2*, Ljung-Box and Diebold-Mariano tests*). Additionally, as a by-product of this study, we estimate sectoral weather elasticities for French energy demand at both monthly and daily levels. These estimations provide a valuable tool for policymakers and researchers, especially for calibrating micro-simulation models used in France.

References

ADEME, 2022. Représentations sociales du changement climatique. Technical Report.

Aghabozorgi, S., Shirkhorshidi, A.S., Wah, T.Y., 2015. Time-series clustering – A decade review. Information systems 53, 16–38. doi:10.1016/j.is.2015.04.007.

Asadoorian, M.O., Eckaus, R.S., Schlosser, C.A., 2008. Modeling climate feedbacks to electricity demand: The case of China. Energy economics 30, 1577–1602. doi:10.1016/j.eneco.2007.02.003.

Atalla, T., Gualdi, S., Lanza, A., 2018. A global degree days database for energy-related applications. Energy 143, 1048–1055.

Bessec, M., Fouquau, J., 2008. The non-linear link between electricity consumption and temperature in Europe: A threshold panel approach. Energy Economics 30, 2705–2721. doi:10.1016/j.eneco.2008.02.003.

Carcedo, J.M., Vicéns-Otero, J., 2005. Modelling the non-linear response of Spanish electricity demand to temperature variations. Energy economics 27, 477–494. doi:10.1016/j.eneco.2005.01.003.

CGDD, S., 2023. Bilan énergétique de la france pour 2022. URL: https://www.statistiques.developpement-durable.gouv.fr/bilan-energetique-de-la-france-pour-2022?rubrique=19&dossier=170. browse on 08/01/2025.

Chan, K., Petruccelli, J.D., Tong, H., Woolford, S.W., 1985. A multiple-threshold AR(1) model. Journal of Applied Probability/Journal of applied probability 22, 267–279. doi:10.2307/3213771.

Chaton, C., 2024. Impact of public policies on the dynamics of energy retrofit and fuel poverty in mainland France. Working Paper doi:10.2139/ssrn.4743235.

Considine, T.J., 2000. The impacts of weather variations on energy demand and carbon emissions. Resource and energy economics 22, 295–314. doi:10.1016/s0928-7655(00)00027-0.

Cui, X., Gafarov, B., Ghanem, D., Kuffner, T.A., 2023. On model selection criteria for climate change impact studies. Journal of Econometrics , 105511doi:10.1016/j.jeconom.2023.105511.

De Azevedo, J.A., Chapman, L., Muller, C., 2015. Critique and suggested modifications of the degree days methodology to enable long-term electricity consumption assessments: a case study in Birmingham, UK. Meteorological Applications 22, 789–796. doi:10.1002/met.1525.

De Dear, R., Brager, G., 2001. The adaptive model of thermal comfort and energy conservation in the built environment. International journal of biometeorology 45, 100–108. doi:10.1007/s004840100093.

Dell, M., Jones, B.F., Olken, B.A., 2014. What Do We Learn from the Weather? The New Climate-Economy Literature. Journal of Economic Literature 52, 740–798. doi:10.1257/jel.52.3.740.

Diebold, F.X., Mariano, R.S., 1995. Comparing predictive accuracy. Journal of Business and Economic Statistics 13, 253–263.

Donovan, J.J., Fischer, W.P., 1976. Factors affecting residential heating energy consumption. Working Paper .

Dubin, J.A., 2008. An integrated engineering–econometric analysis of residential balance point temperatures. Energy economics 30, 2537–2551. doi:10.1016/j.eneco.2007.02.013.

EdF, 2024. L'électricité dans le secteur résidentiel. https://www.edf.fr/groupe-edf/comprendre/electricite-au-quotidien/usages/electricite-dans-le-secteur-residentiel. Accessed: 2024-12-11.

Engle, R.F., Granger, C.W.J., Rice, J.A., Weiss, A., 1986. Semiparametric Estimates of the Relation between Weather and Electricity Sales. Journal of the American Statistical Association 81, 310–320. doi:10.1080/01621459.1986.10478274.

Eskeland, G.S., Mideksa, T.K., 2010. Electricity demand in a changing climate. Mitigation and adaptation strategies for global change 15, 877–897. doi:10.1007/s11027-010-9246-x.

Fazeli, R., Rüth, M., Davíðsdóttir, B., 2016. Temperature response functions for residential energy demand – A review of models. Urban climate 15, 45–59. doi:10.1016/j.uclim.2016.01.001.

Gelegenis, J., 2009. A simplified quadratic expression for the approximate estimation of heating degree-days to any base temperature. Applied energy 86, 1986–1994. doi:10.1016/j.apenergy.2009.02.007.

Giraudet, L.G., Bourgeois, C., Quirion, P., 2021. Policies for low-carbon and affordable home heating: A French outlook. Energy policy 151, 112140. doi:10.1016/j.enpol.2021.112140.

Greevy, J.M., Muguruza, A., Issa, Z., Salvi, C., Chan, J.R., Žurič, Z., 2024. Detecting multivariate market regimes via clustering algorithms. Social Science Research Network doi:10.2139/ssrn.4758243.

Halkidi, M., Vazirgiannis, M., Batistakis, Y., 2000. Quality scheme assessment in the clustering process, in: Principles of Data Mining and Knowledge Discovery: 4th European Conference, PKDD 2000 Lyon, France, September 13–16, 2000 Proceedings 4, Springer. pp. 265–276.

Hekkenberg, M., Moll, H., Uiterkamp, A.S., 2009. Dynamic temperature dependence patterns in future energy demand models in the context of climate change. Energy 34, 1797–1806. doi:10.1016/j.energy.2009.07.037.

Henley, A., Peirson, J., 1997. Non-Linearities in Electricity Demand and Temperature: Parametric Versus Non-Parametric Methods. Oxford bulletin of economics and statistics 59, 149–162. doi:10.1111/1468-0084.00054.

Horvath, B., Issa, Z., Muguruza, A., 2021. Clustering Market Regimes Using the Wasserstein Distance. Social Science Research Network doi:10.2139/ssrn.3947905.

Hurn, A.S., Silvennoinen, A., Teräsvirta, T., 2016. A smooth transition logit model of the effects of deregulation in the electricity market. Journal of Applied Econometrics 31, 707–733.

Isaac, M., Van Vuuren, D., 2009. Modeling global residential sector energy demand for heating and air conditioning in the context of climate change. Energy policy 37, 507–521. doi:10.1016/j.enpol.2008.09.051.

Jäger, J., 1983. Climate and energy systems: A review of their interactions. volume 12. John Wiley & Sons.

Kennard, H., Oreszczyn, T., Mistry, M., Hamilton, I., 2022. Population-weighted degree-days: the global shift between heating and cooling. Energy and Buildings 271, 112315. doi:10.1016/j.enbuild.2022.112315.

Kissock, J.K., Haberl, J., Claridge, D., 2003. Inverse Modeling Toolkit: Numerical Algorithms for Best-Fit Variable-Base Degree Day and Change Point Models. Working Paper .

Labriet, M., 2013. Impacts of Climate Change on Heating and Cooling: A Worldwide Estimate from Energy and Macro-Economic Perspective. Working Paper .

Liao, T.W., 2005. Clustering of time series data—a survey. Pattern recognition 38, 1857–1874. doi:10.1016/j.patcog.2005.01.025.

Lo, M.C., Zivot, E., 2001. Threshold cointegration and nonlinear adjustment to the law of one price. Macroeconomic Dynamics 5, 533–576. doi:10.1017/s1365100501023057.

Lundström, L., 2017. Adaptive weather correction of energy consumption data. Energy Procedia 105, 3397–3402. doi:10.1016/j.egypro.2017.03.778.

MacQueen, J.B., 1967. Some methods for classification and analysis of multivariate observations. Working Paper 1, 281–297.

Mitchell, J.F.B., 1984. Climate and energy systems: A review of their interactions. Quarterly journal of the Royal Meteorological Society 110, 776–777. doi:10.1002/qj.49711046519.

MTE, 2020. Stratégie nationale Bas-Carbonne. Technical Report.

Pang, O., Bell, W., Monsell, B., 2022. Accomodating Weather Effects in Seasonal Adjustment . Working Paper .

Pardo, Meneu, V., Valor, E., 2002. Temperature and seasonality influences on Spanish electricity load. Energy economics 24, 55–70. doi:10.1016/s0140-9883(01)00082-2.

Quartier-La-Tente, A., Michalek, A., Palate, J., Baeyens, R., 2024. Interface to 'JDemetra+' Seasonal Adjustment Software [R package RJDemetra version 0.2.5]. R Package .

Rüth, M., Lin, A.C., 2006. Regional energy demand and adaptations to climate change: Methodology and application to the state of Maryland, USA. Energy policy 34, 2820–2833. doi:10.1016/j.enpol.2005.04.016.

Sailor, D.J., Pavlova, A., 2003. Air conditioning market saturation and long-term response of residential cooling energy demand to climate change. Energy 28, 941–951. doi:10.1016/s0360-5442(03)00033-1.

Sgarlato, R., Ziel, F., 2023. The Role of Weather Predictions in Electricity Price Forecasting Beyond the Day-Ahead Horizon. IEEE transactions on power systems 38, 2500–2511. doi:10.1109/tpwrs.2022.3180119.

Sherman, M.H., 1987. Estimation of infiltration from leakage and climate indicators. Energy and Buildings 10, 81–86. doi:10.1016/0378-7788(87)90008-9.

Sinnott, D., 2016. Dwelling Airtightness: a Socio-technical evaluation in an Irish context. Building and Environment 95, 264–271. doi:10.1016/j.buildenv.2015.08.022.

Staffell, I., Pfenninger, S., Johnson, N., 2023. A global model of hourly space heating and cooling demand at multiple spatial scales. Nature Energy 8, 1328–1344.

Thao Khamsing, W., Ceci-Renaud, N., Guillot, L., 2016. Simuler l'impact social de la fiscalité énergétique : le modèle Prometheus. Working Paper 138.

Thom, H.C.S., 1954. The rational relationship between heating degree days and temperature. Monthly Weather Review 82.

A Appendix

A.1 Litterature review on HDD/CDD

Table 12: Panel of base temperatures found in the literature and associated justifications

Country	Authors	Journal	Base Temperature (°C)	Justifications
Australia	Badescu and Zamfir (1999)	Energy conversion and management	18	18°C is a common base temperature used in the determination of Heating Degree Days
New Zealand	Badescu and Zamfir (1999)	Energy conversion and management	15,6 and 16	-
Romania	Badescu and Zamfir (1999)	Energy conversion and management	18	18°C is a common base temperature used in the determination of Heating Degree Days
United Kingdom	Badescu and Zamfir (1999)	Energy conversion and management	16	-
Israel	Beenstock et al. (1999)	Energy Economics	10	-
Argentina	Castaneda and Claus (2013)	International journal of climatology	18,3	Thom (1954)
United States of America	Considine (2000)	Resource and Energy Economics	18,3	'A degree-day is the difference between a day's average temperature in Fahrenheit and 65°F'
South-Africa	D. Conradie et al. (2018)	Building Research and Information	18	18°C is a common base temperature used in the determination of Heating Degree Days
Italy	De Rosa et al. (2014)	Applied energy	18,3	Thom (1954)
Saudi Arabia	El-Shaarawi and Al-Masri (1996)	Energy	17,8 and 21,1	-
Europe	Eskeland and Mideksa (2010)	Mitigation and adaptation strategies for global change	18 and 22	'A temperature interval is defined as a comfort zone [. . .] i.e., between 18 and 22°C'
Western Europe	Golombek et al. (2012)	Climatic change	18	18°C is a common base temperature used in the determination of Heating Degree Days
Netherlands	Hekkenberg et al. (2009)	Energy Policy	18	18°C is a common base temperature used in the determination of Heating Degree Days
Worldwide	Isaac and Van Vuuren (2009)	Energy Policy	18	18°C is a common base temperature used in the determination of Heating Degree Days
Turkey	Kadioglu et al. (1999)	Applied Meteorology and Climatology	15	18°C is a common base temperature used in the determination of Heating Degree Days
Hong Kong	Lam (1998)	Energy conversion and management	18,3	Thom (1954)
Greece	Papakostas at al. (2010)	Renewable Energy	15	-
Saudi Arabia	Said (1992)	Engineering And Applied Engineering	18 and 21	-
Ireland	Semmler et al. (2010)	Meterological Applications	18	'This temperatures is the most common base temperature of normally insulated buildings'
Europe	Spinoni et al. (2015)	International journal of climatology	15,5	-
United States of America	Taha (1997)	Energy and buildings	18,3	Thom (1954)
Macedonia	Taseska et al. (2012)	Energy	20	-
United States of America	Thom (1954)	Monthly Weather Review	18,3	Derived from a historical temperature probability function
Spain	Valor et al. (2001)	Journal of Applied Meteorology	15	'Within these two limits a comfort zone was established and no heating or cooling is required'
Spain	Valor et al. (2001)	Journal of Applied Meteorology	18	18°C is a common base temperature used in the determination of Heating Degree Days
United States of America	Deschênes and Greenstone (2011)	American economic journal	18,3	Thom (1954)

A.2 Data sources

Table 13: Variables used, sources and transformations

Data category	Variable	Code	Period	Data Source	Original Code	Scale
Energy consumption	Electricity consumption at low tension	conso_elec	01/2000 - 10/2023	French Statistical Data and Studies Department	CONSO_ELEC_BT	TWh
	Electricity consumption at low tension	conso_elec	01/2000 - 10/2023	French Statistical Data and Studies Department	CONSO_ELEC_MT	TWh
	Electricity consumption at low tension	conso_elec	01/2000 - 10/2023	French Statistical Data and Studies Department	CONSO_ELEC_HT	TWh
	Gas distributed consumption	conso_gas	01/2000 - 10/2023	French Statistical Data and Studies Department	CONSO_GAZ_TRANSP	TWh
	Gas transported consumption	conso_gas	01/2000 - 10/2023	French Statistical Data and Studies Department	CONSO_GAZ_DISTRIB	TWh
Weather	Cloudiness	cloudiness	01/2000 - 10/2023	French meteorology and climatology service	NBSIGMA80	Days
	Rainfall	rain	01/2000 - 10/2023	French meteorology and climatology service	RR	Millimeters
	Sunlight	sunlight	01/2000 - 10/2023	French meteorology and climatology service	INST	Minutes
	Temperature	temp	01/2000 - 10/2023	French meteorology and climatology service	TNTXM	°C
	Wind speed	wind	01/2000 - 10/2023	French meteorology and climatology service	FFM	Meters per second
Demography	France total population	pop	2020	National Institute of Statistics and Economic Studies (Insee)	PTOT	Number of individual
Working days	Working days - Week	reg2_ac1	01/2000 - 10/2023	National Institute of Statistics and Economic Studies (Insee)	REG2_AC1	
	Working days - Week-end	reg2_ac2	01/2000 - 10/2023	National Institute of Statistics and Economic Studies (Insee)	REG2_AC2	
	Leap year	ly	01/2000 - 10/2023	National Institute of Statistics and Economic Studies (Insee)	LY	

A.3 Descriptive statistics

A.3.1 Monthly data

Figure 11: ACF and PACF for electricity and natural gas consumption

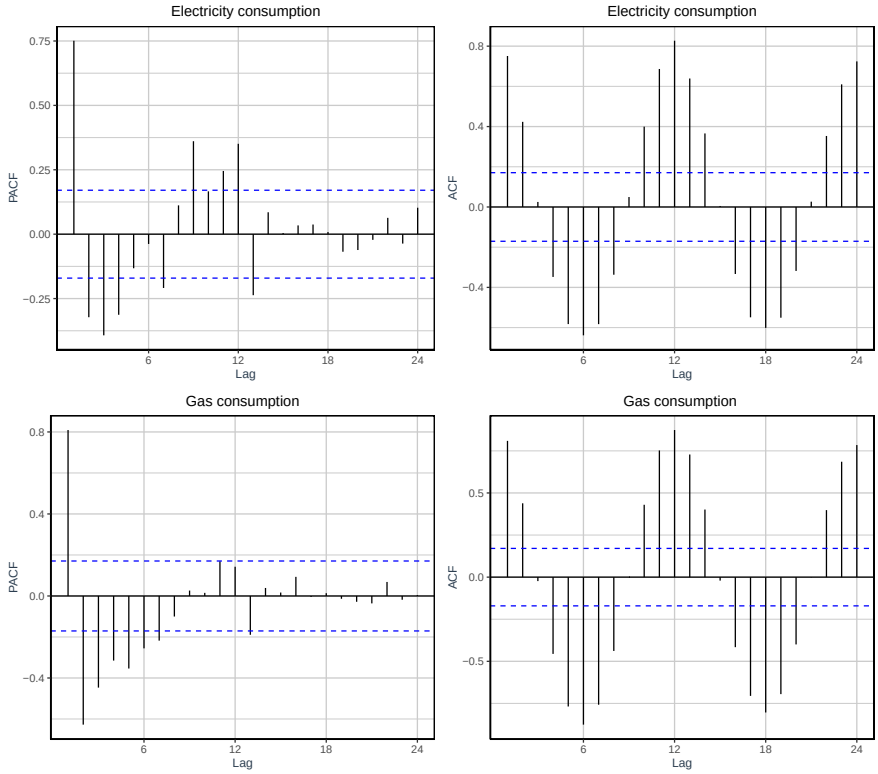

Table 14: Descriptive statistics of demand (TWh)

	N	Mean	St. Dev.	Min	Max
$q_t^{Low_g}$	132	21.99	14.36	4.79	53.89
$q_t^{High_g}$	132	13.00	3.08	7.67	20.17
$q_t^{Low_e}$	132	16.01	5.04	10.55	27.86
$q_t^{Med_e}$	132	13.20	1.06	9.84	16.27
$q_t^{High_e}$	132	6.52	0.49	4.73	7.49
q_t^{gas}	132	34.98	16.96	13.32	73.29
q_t^{elec}	132	35.74	6.17	27.68	51.54

Notes : The descriptive statistics are reported as TWh consumption. The variables q_t^{gas} and q_t^{elec} represent the sums of the respective variables $q_t^{Low_g}$, $q_t^{High_g}$ and $q_t^{Low_g}$,$q_t^{Med_g}$,$q_t^{High_g}$. The monthly data spans the period from January 2019 to December 2022.

Table 15: Share of economic sector regarding the energy delivery mode - Median

	Residential	Service	Industrial	Other	Total
$q_t^{Low_e}$	79,6%	16,0%	1,5%	2,9%	100%
$q_t^{Med_e}$	0,0%	57,5%	39,0%	3,3%	100%
$q_t^{High_e}$	0,0%	18,8%	81,2%	0,0%	100%
$q_t^{Low_g}$	46,4%	26,2%	27,2%	1,3%	101%
$q_t^{High_g}$	0,0%	6,2%	93,8%	0,0%	100%

Notes : The table presents the breakdown of energy consumption by delivery mode into the sectorial consumption mode. This distribution rely on a SDES annual survey of energy suppliers and is computed on the 2018-2022 vintage.

Table 16: Share of delivery mode for each energy demand - Median

	$q_t^{Low_e}$	$q_t^{Med_e}$	$q_t^{High_e}$
q_t^{Elec}	43.44%	35.23%	21.33%
	$q_t^{Low_g}$		$q_t^{High_g}$
q_t^{Gas}	64.62%		35.38%

Notes : The table presents the breakdown of aggregate energy demand time series regarding the delivery mode.

A.3.2 Daily data

Figure 12: Daily electricity consumption in TWh

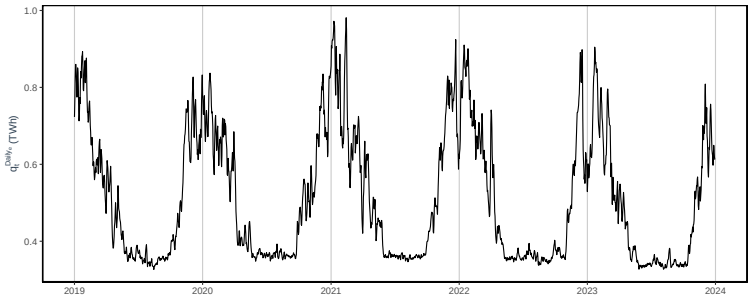

Figure 13: ACF and PACF for daily electricity consumption

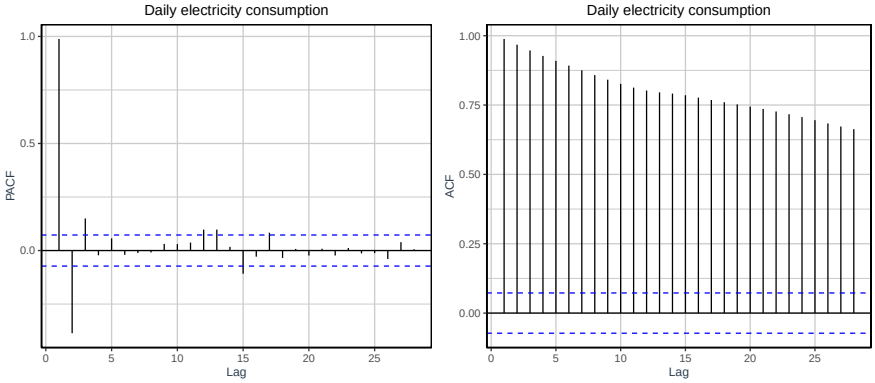

Table 17: Descriptive statistics electricity demand (< 36 kVA) in TWh

	N	**Mean**	**St. Dev.**	**Min**	**Max**
$q_t^{Daily_e}$	1461	0.524	0.168	0.327	0.981
$q_t^{Monthly_e}$	36	15.95	4.87	10.64	26.22
q_t^{Low}	36	15.92	4.88	10.59	26.04

Notes : The table presents the data distribution at the daily level $q_t^{Daily_e}$ for the 1096 days available on the dataset. The same statistics are computed at the monthly aggregate level $q_t^{Monthly_e}$ on the series and compared with the $q_t^{Low_e}$ monthly series from the main study. Both series from different sources and on different time frames describe similar energy consumption behaviour.

Table 18: Correlation between weather indicators and energy time series - Daily data

	temp	**sunlight**	**wind**	**rain**
$q_t^{Daily_e}$	-0.912	-0.548	0.221	0.042
	(0.000)	(0.000)	(0.000)	(0.162)

Notes : The table show the correlation coefficients and the p-value associated in brackets. The p-values represent the probability that the null hypothesis, which represents a null correlation, is non-rejected. Thus a null p-value is interpreted as a correlation significantly different from 0.

A.3.3 Daily regional data

Figure 14: France 12 administrative regions

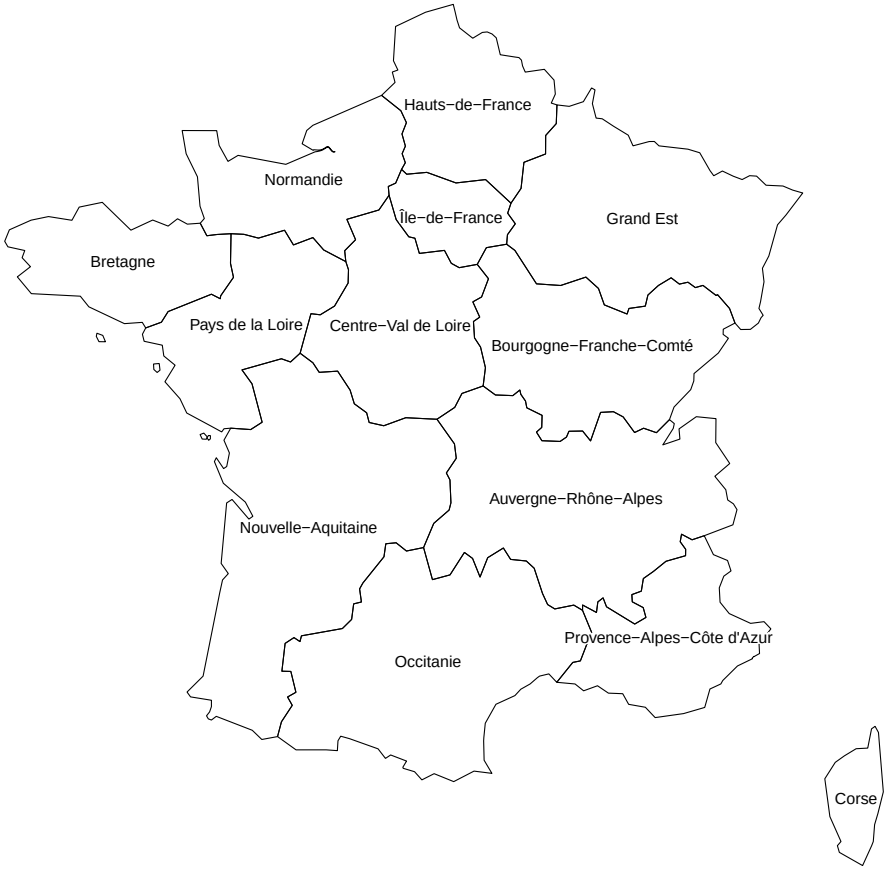

Authors design, 2024
Bruguet, Thomas, Le Saoult

Table 19: Descriptive statistics regional electricity demand (< 36 kVA) in TWh

	N	Mean	St. Dev.	Min	Max
Centre-Val de Loire	730	0.021	0.008	0.013	0.041
Bourgogne-Franche-Comté	730	0.022	0.007	0.015	0.042
Normandie	730	0.028	0.011	0.017	0.057
Bretagne	730	0.029	0.011	0.018	0.058
Grand Est	730	0.031	0.010	0.020	0.056
Pays de la Loire	730	0.032	0.012	0.020	0.063
Hauts-de-France	730	0.039	0.013	0.024	0.074
Provence-Alpes-Côte d'Azur	730	0.048	0.014	0.032	0.086
Nouvelle-Aquitaine	730	0.050	0.017	0.033	0.096
Occitanie	730	0.052	0.017	0.035	0.100
Auvergne-Rhône-Alpes	730	0.063	0.021	0.042	0.122
Île-de-France	730	0.074	0.025	0.043	0.138

Notes : The table presents the data distribution at the daily level for 12 different regions and for the 730 days available on the dataset. The region "*Centre-Val de Loire*" is the one with the lowest mean consumption over a day, with 0.021 TWh and the region "*Ile-de-France*" is the one with the highest mean consumption over a day with 0.074TWh.

Table 20: Correlation between weather indicators and energy time series - Daily regional data

	temp	sunlight	wind	rain
Île-de-France	-0.906	-0.493	0.168	-0.010
	(0.000)	(0.000)	(0.001)	(0.848)
Centre-Val de Loire	-0.897	-0.522	0.181	-0.097
	(0.000)	(0.000)	(0.001)	(0.065)
Bourgogne-Franche-Comté	-0.904	-0.494	0.182	-0.085
	(0.000)	(0.000)	(0.000)	(0.105)
Normandie	-0.891	-0.484	0.205	0.038
	(0.000)	(0.000)	(0.000)	(0.467)
Hauts-de-France	-0.899	-0.494	0.183	0.015
	(0.000)	(0.000)	(0.000)	(0.780)
Grand Est	-0.911	-0.529	0.214	-0.045
	(0.000)	(0.000)	(0.000)	(0.393)
Pays de la Loire	-0.875	-0.500	0.119	0.016
	(0.000)	(0.000)	(0.023)	(0.767)
Bretagne	-0.870	-0.493	0.111	0.101
	(0.000)	(0.000)	(0.034)	(0.055)
Nouvelle-Aquitaine	-0.866	-0.391	0.056	0.011
	(0.000)	(0.000)	(0.285)	(0.839)
Occitanie	-0.826	-0.345	0.063	0.047
	(0.000)	(0.000)	(0.233)	(0.367)
Auvergne-Rhône-Alpes	-0.888	-0.484	0.018	-0.087
	(0.000)	(0.000)	(0.732)	(0.098)
Provence-Alpes-Côte d'Azur	-0.784	-0.329	0.145	0.002
	(0.000)	(0.000)	(0.005)	(0.970)

Notes : The table show the correlation coefficients and the p-value associated. The p-values represent the probability that the null hypothesis, which represents a null correlation, is non-rejected. Thus a null p-value is interpreted as a correlation significantly different from 0.

A.4 Ordered energy consumption and weather variables

Figure 15: $q_t^{Low_e}$ demand as a function of weather

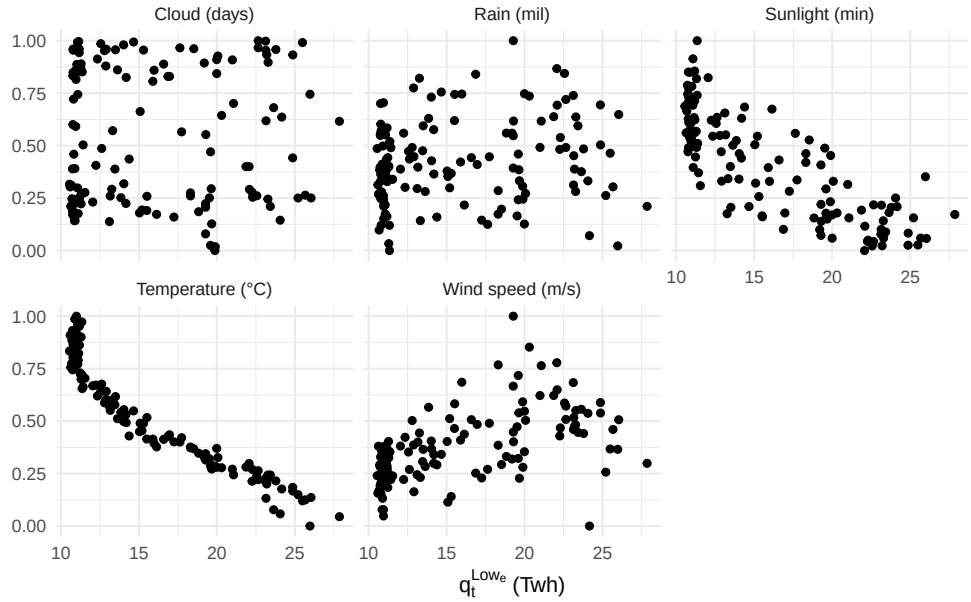

Notes : Normalized visualisation of energy demand with regards to weather variables.

Figure 16: $q_t^{Med_e}$ demand as a function of weather

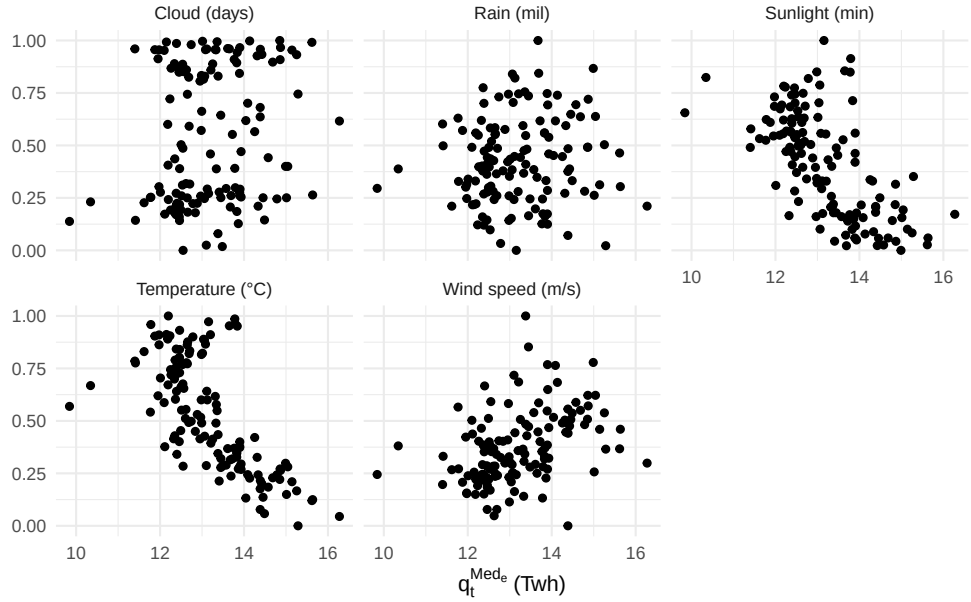

Notes : Normalized visualisation of energy demand with regards to weather variables.

Figure 17: $q_t^{High_e}$ demand as a function of weather

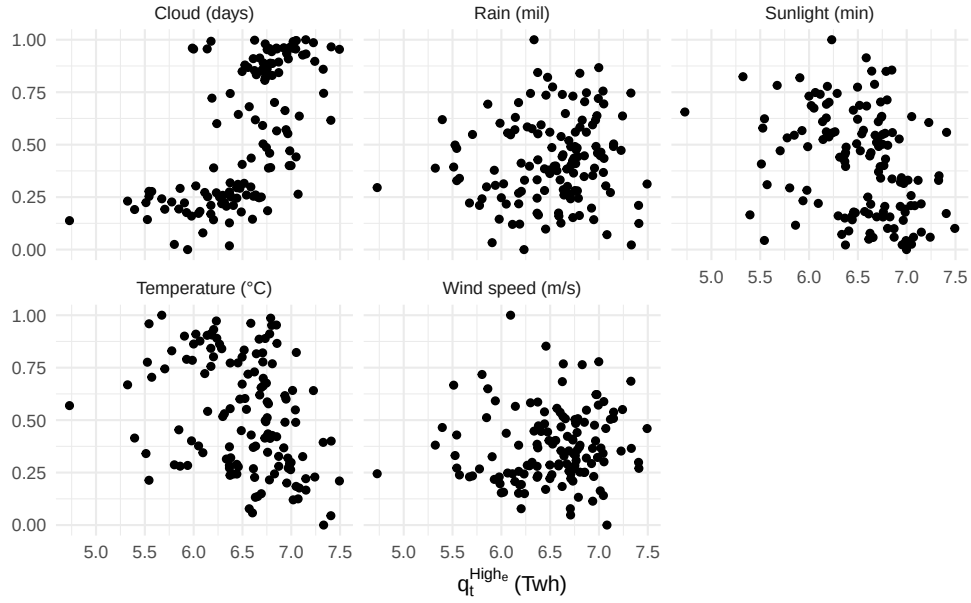

Notes : Normalized visualisation of energy demand with regards to weather variables.

Figure 18: $q_t^{Low_g}$ demand as a function of weather

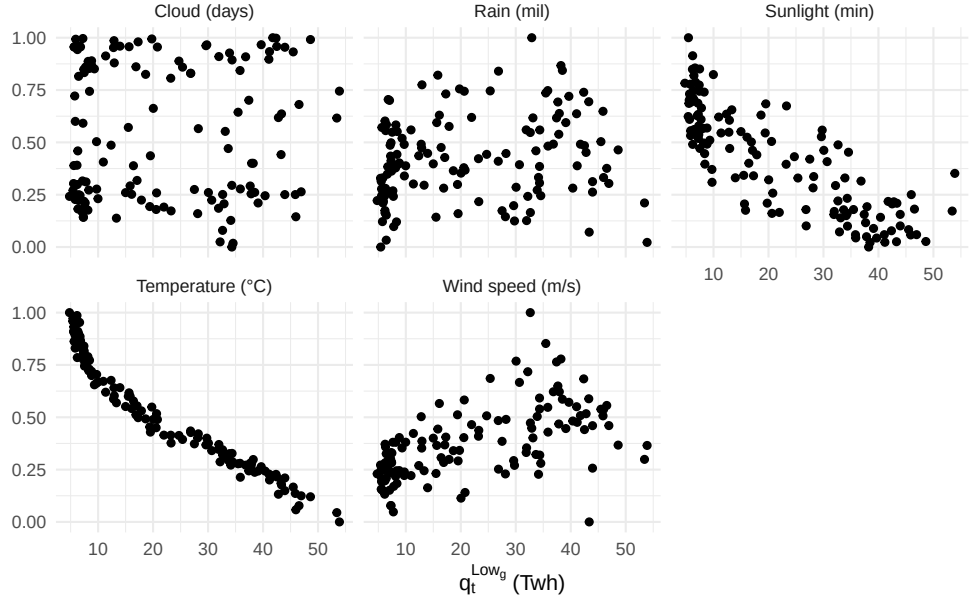

Notes : Normalized visualisation of energy demand with regards to weather variables.

Figure 19: $q_t^{High_g}$ demand as a function of weather

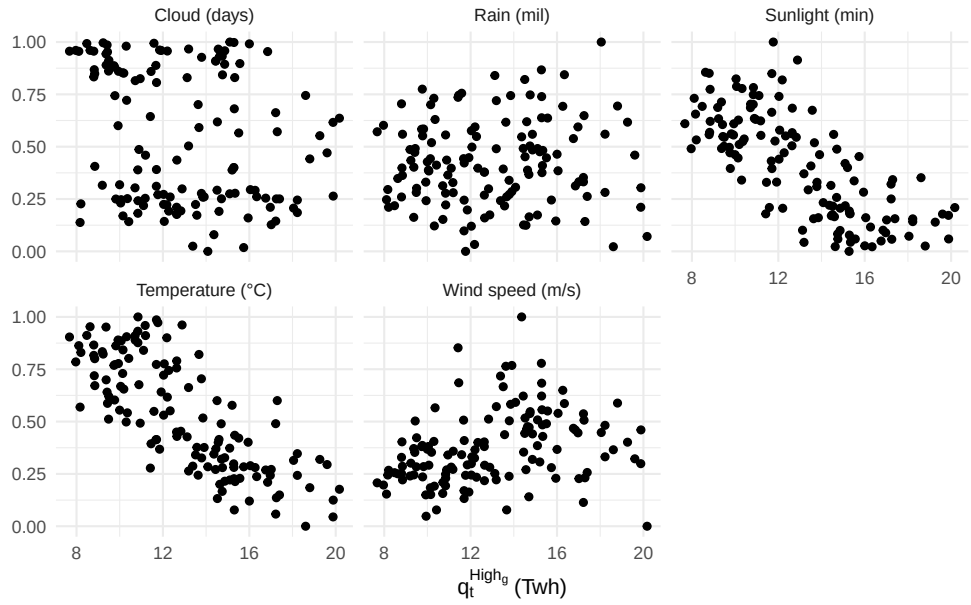

Notes : Normalized visualisation of energy demand with regards to weather variables.

A.5 Procedure to define the number of centroïds

Figure 20: Detection of the optimal number of cluster via the SDindex

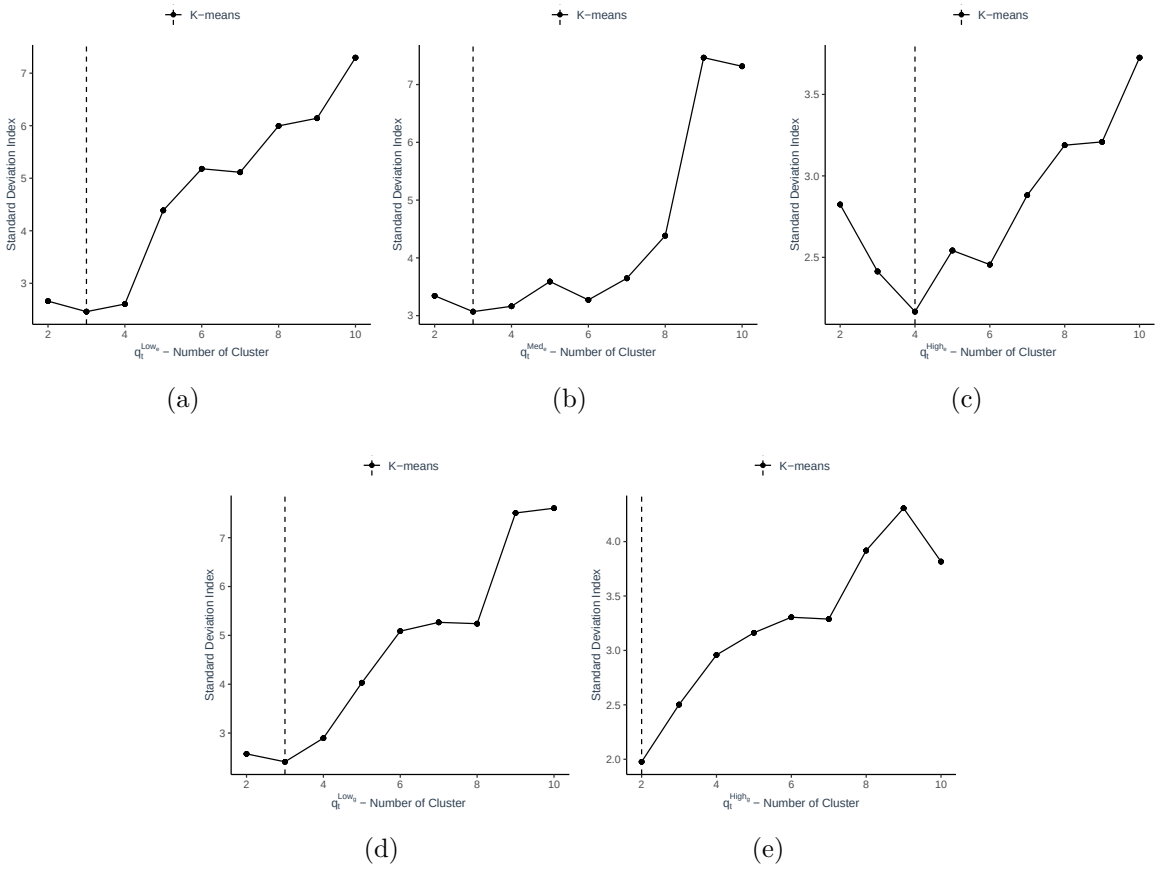

Notes: The figures showcase the level of the *Standard Deviation Index* relative to the number of clusters. The dotted vertical line highlight the number of cluster that allow to minimize the index and thus define the optimal number of cluster.

A.6 Dubin (2008) functional form with two heating thresholds

Figure 21: Functional form adapted from Dubin (2008)

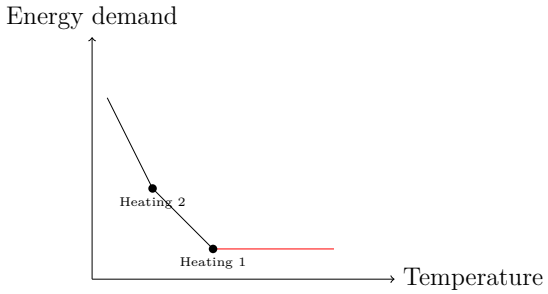

B Complementary results

B.1 Weights sources

To test the robustness of weighting solely by population, we explored weighting by employment rates. Specifically, employment in the industrial sector was used for industrial energy demand, while employment in non-industrial sectors was used for the service sector.

To evaluate the impact of these alternative weighting methods, we analyze the distribution of weighted temperatures graphically (see Figure 22) and conduct Wilcoxon significance tests (see Table 21). In all comparisons, the p-values are significantly greater than the typical significance threshold, indicating that the null hypothesis of no difference in the location of the distributions could not be rejected. These findings suggest that the distributions of the differently weighted temperatures are statistically similar.

Table 21: Wilcoxon rank sum test results

Comparison	W Statistic	p-value
Population vs Workplace	37 617	0.8017
Population vs Industrial	39 073	0.5993
Industrial vs Workplace	36 773	0.4829

Notes: The table showcase the Wilcoxon statistics and the associated p-value. Since the Wilcoxon test is bilateral, we conducted three combinations of bilateral tests to comprehensively cover all necessary comparisons for determining significant results regarding mean differences.

Figure 22: Monthly mean weighted temperature distributions

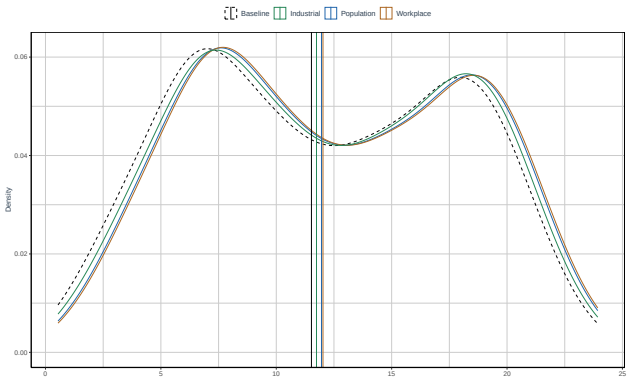

Notes: The figure illustrates the monthly mean weighted temperature distributions across four different contexts: Baseline (non weighted), Population (weighted by population distribution), Workplace (weighted by workplace proxy by non industrial employment) and Industrial (weighted by industrial activity proxy by industrial employment). Solid vertical lines indicate the median for each distribution. Daily temperature data spans the period from January 2000 to December 2022.

B.2 Cluster detection for *Provence-Alpes-Côte d'Azur*

Figure 23 presents the relationship between temperature and electricity demand for two different regions namely *Provence-Alpes-Côte d'Azur* (a) and *Bourgogne-France-Comté* (b). Each panel shows clustering results based on temperature thresholds identified by the clustering algorithm. The dashed vertical lines represent the detected thresholds, and each cluster is displayed with distinct colors or shades. Panel (b) serves as a reference, as it closely resembles the national-level relationship between temperature and electricity demand. This figure reveals a known L-shaped curve with three clusters: electricity demand decreases with rising temperatures up to a certain threshold, after which it stabilizes at low levels. In contrast, Panel (a) highlights a region with a specific demand response during the summer months, apriori driven by the use of air conditioning. Here, the clustering algorithm detects five distinct clusters and reflecting a U-shape relationship between temperature and electricity demand. Notably, at higher temperatures, the demand increases again due to air conditioning use, which diverges from the behavior observed at the national scale. This comparison illustrates the heterogeneity in temperature sensitivity across regions, with regional-specific factors, such as the prevalence of cooling systems, influencing the shape of the temperature-demand relationship.

Figure 23: Regional clustering analysis of energy response to temperature

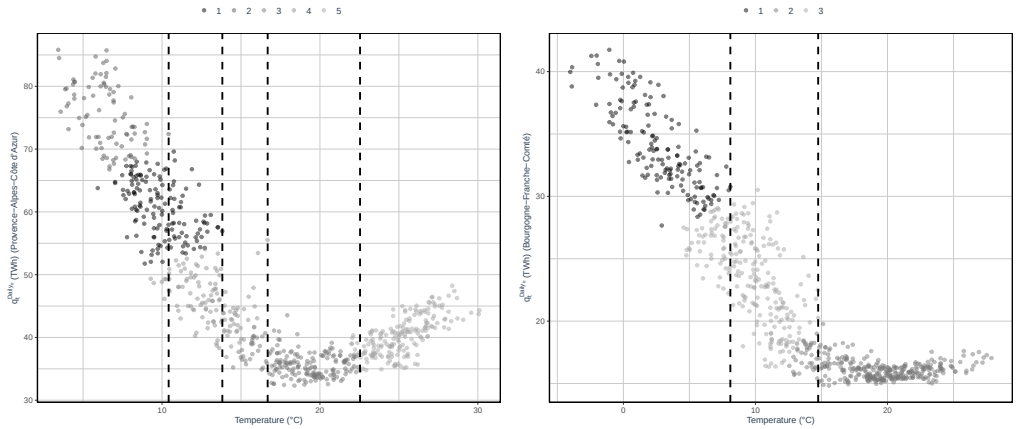

(a) (b)

Notes: These figures are a visual representation of the K-means algorithm results. The dashed lines represent the regime-switching point, or base temperature and the clusters represent the different regimes. Daily regional energy consumption and weather data span the period from January 2019 to December 2022.

B.3 Threshold detection via SETAR procedure

A seminal methodology was to draw upon Carcedo and Vicéns-Otero (2005) and Bessec and Fouquau (2008), which employs a Smooth Transition AR (STAR) method based on a predetermined definition of the data generation function. However, a smooth method induces to define a priori the function that best describes the relation between the series. Since we want our method to be also useful for other indicators than the temperature, our proposal relies on the adoption of a non-smooth methodology grounded in the method of multivariate Threshold Vector Autoregression (TVAR) from Lo and Zivot (2001) and based on the Self-extracting AR (SETAR) modelling paradigm.

A TVAR model extends the traditional VAR framework by incorporating threshold effects, allowing for nonlinear dynamics in the relationships between variables. This approach is particularly useful when the relationships between variables are subject to structural changes or regime shifts. In a multivariate TVAR model, the data is divided into different regimes or states, and separate VAR models are estimated for each regime. The key feature of a multivariate TVAR model is the identification of thresholds that determine the switch between different regimes. For reference, in a univariate dimension, the SETAR modelling with two regimes and one threshold can be describe as in (9) and allows to estimate the coefficients ϕ_1 and ϕ_2 but also the threshold c that correspond to the transition between both regimes.

$$z_t = \begin{cases} \phi_1 z_{t-1} + \epsilon_{1t} & \text{if } z_{t-1} \leq c \\ \phi_2 z_{t-1} + \epsilon_{2t} & \text{if } z_{t-1} > c \end{cases} \tag{9}$$

Estimating the threshold parameter is not obvious due to its representation as a discontinuous function. A viable approach involves concentrating the objective function since the slope estimators given a known threshold can be estimated by ordinary least squares (OLS), the problem can be simplified by concentrating out the minimization problem through $\phi(\Theta)$ and the corresponding sum of squares SSR(Θ). This leads to the following objective function:

$$\hat{\Theta} = \arg\min_{\Theta} SSR(\Theta) \tag{10}$$

Minimization of (10) is done through a grid search: values of the threshold are sorted, the SSR is estimated for each selected threshold and the one that minimize the SSR is taken as the estimator. Table 22 showcases thresholds levels estimated with this first method.

Table 22: General Weather Indicator - Step 1 based on SETAR

	Temperature	**Wind**	**Sunlight**	**Rain**	**Cloudiness**
$q_t^{Low_g}$	11; 15	3.2	281; 395	1.5; 2	25
$q_t^{High_g}$	10; 15.5	3; 3.5	286; 395	2	23
$q_t^{Low_e}$	10; 15	3; 3.5	323; 412	2	24
$q_t^{Med_e}$	13; 19	3; 3.5	379; 461	2	24
$q_t^{High_e}$	13; 16	3; 3.5	286; 395	2	24

Notes: Extracted thresholds w_{base} using the SETAR procedure. Monthly energy consumption and weather data span the period from January 2012 to December 2022.